CHAPTER VI

Microporous Membranes of Polyoxymethylene from a Melt-Extrusion Process: (II) Effects of Thermal Annealing and Stretching on Porosity

ABSTRACT

A two part study utilizing polyoxymethylene (POM) was undertaken to investigate a three stage process (melt-extrusion/annealing/uniaxial-stretching) (MEAUS) utilized to produce microporous films. In this report, the thermal annealing (second stage) and subsequent uniaxial-stretching (third stage) results of selected POM films from two commercial resins, labeled D & F, are discussed. Specifically, the annealing and uniaxial stretching effects on film morphology, orientation, and other pertinent film properties are addressed. Additionally, sequential analysis was performed regarding the influence each stage had on the resulting microporosity. It was found that the melt-extruded precursor morphology and orientation, as a consequence of the first stage extrusion parameters and resin characteristics, are crucial to controlling the membrane permeability. The annealing parameters were also deemed critical, where a temperature of 145°C applied for 20 min. under no tension was the optimum annealing condition for producing a highly microporous film upon stretching. For the conditions studied, the stretching parameters that were found to be optimum for producing the desired characteristics in the final film were a cold temperature of 50°C and hot stretch temperature of 100°C. The optimum extension levels were concluded to be 90 percent for both the cold and hot stretch steps and thus a total overall extension level of 180 percent. However, these results were only with respect to resin F films. Since the resin D melt-extruded precursors possessed twisted lamellar morphologies and relatively low crystal orientation, its samples could not be produced into microporous films via the MEAUS process.

6.1 INTRODUCTION

This report describes the second portion of a two-part study regarding a process composed of three stages (melt-extrusion/annealing/uniaxial-stretching) (MEAUS) utilized to make microporous membranes. As discovered in our previous sequential investigation[1,2] of the MEAUS process where isotactic poly(4-methyl-1-pentene) (PMP) was utilized, the melt-flow behavior and its orientation prior to crystallization play critical roles in the formation of the morphological features and orientation of the crystallized film. From that study, it was concluded that a parallel planar lamellar morphology possessing a relatively high crystalline orientation are the desirable structural elements for a melt-extruded precursor to possess. This type of lamellar arrangement is clearly a consequence of a row-nucleated morphology created by the appropriate melt-extrusion conditions.

In the first paper of this two part series,[3] the melt-extrusion results of three polyoxymethylene (POM) resins (D, E & F) were reported. Resins D and E differed mainly in weight average molecular weight (M_w) where resin D had a higher value, yet both resins were characterized by relatively narrow molecular weight distributions (MWD) ca. 2. In contrast, resin F possessed a broader MWD (ca. 5.9) and a slightly lower M_w in comparison with resin D. Additionally, the broader MWD resin contained a small amount of ethylene oxide comonomer while the other resins did not contain comonomer. Upon controlled melt-extrusion, resin F precursors generally possessed parallel planar lamellar textures, for the processing window considered. However, resin D or E samples were characterized by twisted lamellae that were arranged into oriented sheaf-like structures, and in some films, spherulitic-like morphologies predominated. Further, the crystalline orientation, as determined via wide-angle X-ray scattering (WAXS), was lowest for resin E specimens followed by those of resin D while resin F samples had the highest orientations. The results were attributed to the process conditions and melt-relaxation time differences between resins, where resin F possessed the longest melt-relaxation time, followed by resin D and resin E, respectively.

The use of annealing (second stage) to promote structural modifications such as lamellar thickening and perfection in the melt-extruded precursor has also been considered important for the formation of microporous membranes made by the MEAUS process.[2,4] This has been accomplished through control of the annealing temperature (T_a), annealing time (t_a), and tension level (percent extension) during annealing. A requirement enabling crystalline thickening and perfection is the occurrence of chain axis crystalline mobility. The thermal transition attributed to this is conventionally denoted as the α_c relaxation.[5,6] As has been recognized, the existence of

such a relaxation is "necessary, but not sufficient"[7] for lamellae to thicken, where the presence of noncrystallizable units along the polymer backbone (comonomer, branches, etc.), highly entangled interlamellar regions, and the nature of the morphology may affect the crystalline thickening process. The end effect is that the lamellae may not thicken sufficiently if such imperfections exist. The comonomer effect on lamellae thickening may have important implications to this study as will be discussed later.

The presence of the α_c relaxation is also believed to be important with respect to the third stage of the MEAUS process, i.e. uniaxial-stretching stage, which is composed of two stretching steps followed by a thermal-relaxation/heat-setting step. The first stretching step is designated the "cold" stretch while the second is the "hot" stretch. The cold stretch temperature (T_{cs}) generally occurs above the polymer T_g but below the hot stretch temperature (T_{hs}), which itself is below the annealing temperature of the prior stage but still in the upper temperature range of the α_c relaxation. The extension levels utilized during the cold stretch (%CS) and hot stretch (%HS) steps also must be examined. The stretching directions in both steps are along the MD of the annealed film, i.e., perpendicular to the stacked lamellae. The cold stretch step is utilized to "nucleate" or initiate the micropores while hot stretching increases their overall pore size. It is in the latter step, hot stretching, that crystalline mobility is believed to enable greater extension levels and thus greater lamellar separation results if an α_c relaxation exists. The thermal-relaxation/heat-setting step is utilized to allow partial recovery and impart dimensional stability to the film after removal from the stretching apparatus.

This sequential study of the MEAUS process addresses the findings with respect to POM. While POM has been shown to form microporous films,[8,9] it has not been followed sequentially with the goal of producing microporous membranes. It is desired that the information obtained from this study will lend itself to understanding the formation of microporous materials via the MEAUS process. Additionally, the results are hoped to facilitate an improved working knowledge of the mechanisms behind each stage, i.e., melt-flow behavior during melt-extrusion, structural modifications occurring while thermal annealing, and the deformation processes taking place during stretching. This will be accomplished by consecutive analysis of the results from each of the three process stages. The findings of the first stage (melt-extrusion) utilizing POM have already been presented[3]. In this second portion of the investigation, the annealing (second stage) and stretching (third stage) effects on POM film morphology, crystal orientation, and other pertinent properties are presented and discussed. Also, the same sample designation as utilized in part 1 will be employed for continuity. Specifically, in this report, we will address

samples, D1, F1, F2, and F3, that were extruded under the conditions stated in Tables 1 and 3 from reference 2. These POM melt-extruded precursor films were chosen based upon their morphological features and orientation state in order to investigate the effects of specific annealing (T_a, t_a & tension) and stretching process variables (T_{cs}, %CS, T_{hs} & %HS).

6.2 EXPERIMENTAL

Materials

The precursor films from two resins (D & F) were utilized in this annealing and stretching investigation. The commercial resin D was a result of anionic polymerization of formaldehyde and end-capping the chains using acetic anhydride. The acetic anhydride was employed to stabilize the chain because POM has a relatively low ceiling temperature (ca 120°C) and the chain undergoes depolymerization (unzipping) initiated at the hydroxyl end groups without end-capping. Resin F was polymerized via a ring-opening polymerization mechanism. This particular synthesis utilizes a small amount of the comonomer ethylene oxide to provide thermal stability to the POM chain.[10] More information addressing the resin characteristics is provided in Table 6.1.

Table 6.1 Molecular weight characteristics for the two POM resins studied.

Resin	M_n (kg/mol)	M_w (kg/mol)	M_w / M_n	T_m (°C)
D	106	195	1.8	178
F	28.0	165	5.9	167

Structural and Optical Techniques Utilized

Wide-Angle X-ray Scattering (WAXS)

WAXS studies were performed on a Philips table-top x-ray generator model PW1720 equipped with a standard vacuum sealed Warhus photographic pinhole camera. The X-ray beam was of Cu Kα radiation, λ = 1.544 Å, and was collimated to a beam diameter of 0.020 inches (0.508 mm).

As previously reported[3], the extrusion lead to planar extensional flow along the MD, this promoted uniaxial orientation behavior with respect to the MD axis. As a result, the nature of the crystalline orientation (orientation function) need only be obtained by examination of the azimuthal angle dependence of appropriate reflections arising from standard flat plate WAXS patterns. The orientation function utilized was the Hermans' orientation function (f_H),[11]

$$f_H = \frac{(3 \cdot \overline{cos^2 \theta} - 1)}{2} \qquad \text{(Eqn. 6.1)}$$

where θ is the angle between the chain or specific unit cell axis and a chosen reference axis, MD. The procedural details for determining the crystalline orientation (f_c) in the POM films discussed in this paper has been given in our first report[3].

Small-Angle X-ray Scattering (SAXS)

SAXS was utilized to estimate the long spacing of the POM precursors. A slit collimation of dimensions 0.03 x 5mm was employed with a Kratky camera using nickel filtered Cu Kα radiation of wavelength 1.544 Å. The SAXS profiles were obtained by passing the beam along the normal direction (ND) to the film and obtaining the scan along the machine direction (MD). No desmearing of the slit-smeared intensity data was undertaken in this investigation. After correction for parasitic scatter was performed using a Lupolen standard, the scattering curves were normalized to the incident intensity and sample thickness. This corrected intensity, **I**(**s**), was plotted against the angular variable,

$$\mathbf{s} = \mathbf{2(\sin\frac{\theta}{2})/\lambda} \qquad \text{(Eqn. 6.2)}$$

where θ is the radial scattering angle. The long period was estimated by using the equation $\ell = 1/\mathbf{s^*}$, where $\mathbf{s^*}$ is the value of **s** at the peak of the slit-smeared **I**(**s**) versus **s** plot. A "heterogeneity index" of the lamellar distribution in the structure was evaluated by determining the full peak width at half the maximum height (Δw) of the first order scattering intensity peak.

Atomic Force Microscopy (AFM)

AFM micrographs were obtained with the use of a Digital Instruments Nanoscope III Scanning Probe Microscope operated in TappingMode™. Nanosensor TESP single beam cantilever tips possessing force constants of 35±7 N/m and oscillated at frequencies of ca. 290 kHz were used. The films were placed upon glass slides using double stick tape with raster-scanning parallel to film MD.

Differential Scanning Calorimetry (DSC)

DSC measurement was performed with a Perkin-Elmer DSC-7. Heating scans were conducted utilizing the procedures presented in the POM melt-extrusion report[3].

Dynamic Mechanical Spectroscopy (DMS)

Dynamic mechanical testing was carried out on a Seiko DMS 210. The samples were tested in tensile mode using samples approximately 0.0254 mm thick, 10 mm long, 6 mm wide. The DMS experiments were performed at a frequency of 1Hz using a heating rate of 2°C/min under an N_2 atmosphere.

Gurley Instrument and Film thickness

Film porosity was determined by measuring the stretched film permeability given in terms of the Gurley number, which is the time required for 10cc of air to pass through the 1 inch square section of film at a constant pressure of 12.2 inches of H_2O. The Gurley number measurements are performed using a Gurley densometer model no. 4150. Final films with measured Gurley values less than 100 sec. will be considered "quality" membranes. All Gurley numbers reported in this paper arise from an average of a *minimum* of six measurements made for each sample. Film thickness measurements were carried out on a Series 400 Precision Micrometer.

6.3 RESULTS

As already mentioned, four POM melt-extruded precursors, F1, F2, F3, and D1, were utilized for this study. All four films possessed stacked lamellar morphologies that were in some cases planar. Table 6.2 provides this information along with other pertinent film characteristics. Since the overall goal was to produce POM microporous film, the resin F films were the main focus in this report because these samples possess planar lamellar morphologies and the highest f_c values of any POM films presented in the previous report[3]. However, the reader will recall that resin F was polymerized with the comonomer ethylene oxide while resins D and E were not. Thus, film D1 was selected for comparison purposes because it possessed the most planar lamellar morphology and highest f_c of any resin D or E sample. The comonomer effect can be seen in the lower T_m, X_c, and SAXS long spacing (ℓ) of the resin F precursors relative to those of sample D1, as displayed in Table 6.2.

Table 6.2 Pertinent characteristics for the melt-extruded films F1, F2, F3, & D1.

Sample	Lamellar Morphology	f_c	X_c (%)	T_m (°C)	ℓ (Å)	Δw (nm^{-1})
F1	Partially Twisted	0.81	48	165	128	0.47
F2	Partially Twisted	0.75	48	165	129	0.46
F3	Partially Twisted	0.65	47	166	128	0.47
D1	Sheaf-like/Twisted	0.45	52	178	153	0.51

6.3-1 Annealing:

Because of the large number of annealing and stretching variable combinations utilized, only selected results will be presented here that are, in general, representative of most POM films studied by the authors. The annealing temperatures utilized were chosen based upon the range of temperatures encompassing the POM mechanical α_c relaxation, expressed by Tan δ in Fig. 6.1. From this figure, the α_c relaxation associated with the precursor F1 is observed to range from ca. 40 to 165°C while the temperature range is noted to be approximately 40-175°C for precursor D1. The temperature associated with the maximum value of the α_c, $T_{\alpha c}$, is ca. 120°C for the resin F precursors and ca. 138°C for the resin D precursor. These specific values are of possible importance because Rault[6] has suggested that effective annealing temperatures must be greater than the respective $T_{\alpha c}$ in order for crystal thickening to occur. To investigate this supposition, annealing temperatures of 85, 110, 130, 145, and 150°C were employed for the resin F films while temperatures of 85, 120, 145, 155, and 160°C were used in the limited study of the resin D sample.

Annealing times of 5, 10, and 20 min were used in light of feasible industrial processing times and to provide continuity with our previous MEAUS investigation of PMP[2]. The final annealing variable investigated was the tension level (percent extension) applied to the film. The tension level was divided into two main categories: annealing without tension (free-anneal or 0% tension) and annealing under a specified tension level. In the case of the latter, the tension levels were 3, 9, and 15 percent. The specific level was applied during the annealing stage with a small mechanical stretching apparatus that was also employed in the stretching stage. The specific levels of 3, 9, and 15 percent tension were based upon the previous work of Yu[12] on linear high density polyethylene (HDPE) films and our investigations of PMP films[1,2].

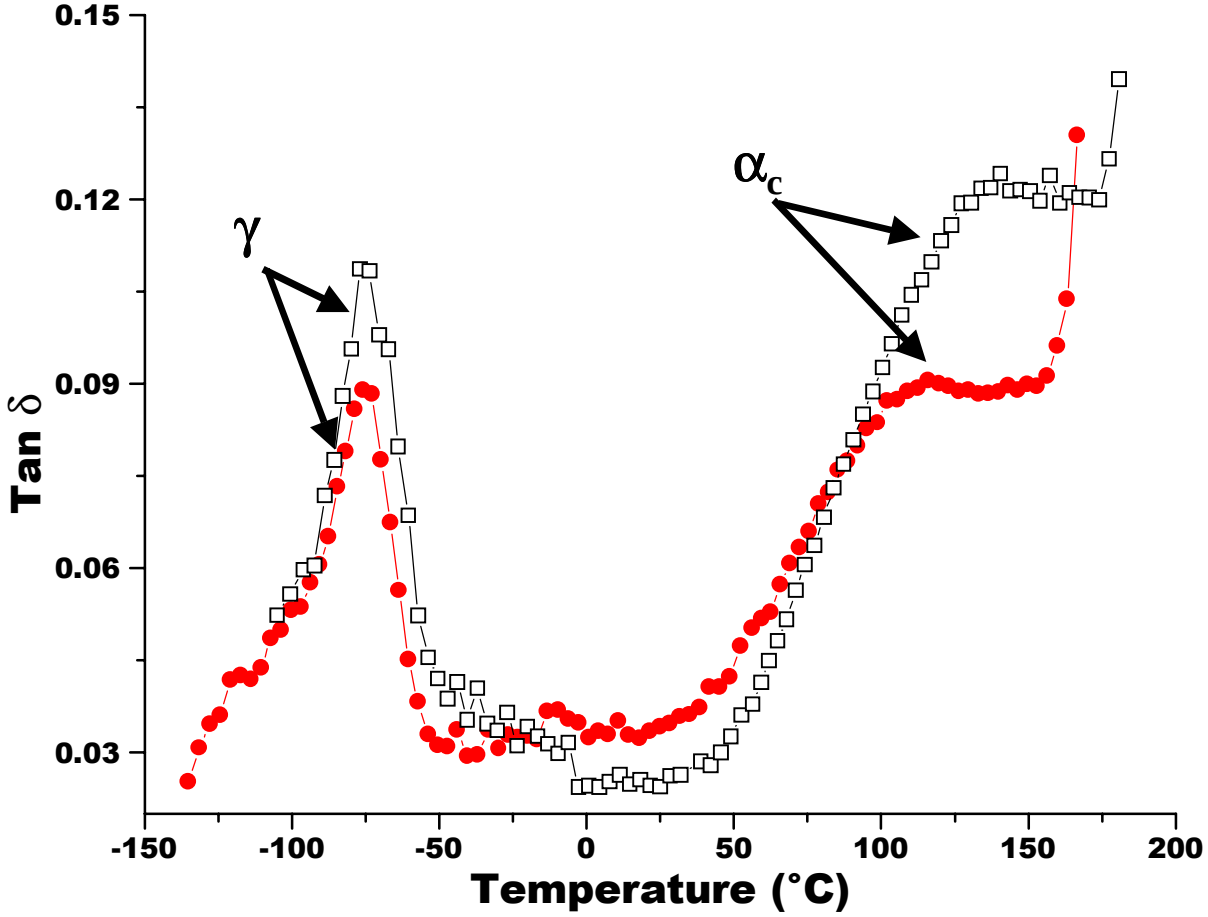

Figure 6.1 Tan δ as a function of temperature for POM films (-□-) D2 and (-●-) F2 with their corresponding γ and α_c relaxations labeled. This data was obtained utilizing a heating rate of 2°C/min and a frequency of 1.0 Hz.

As mentioned, the utility of the annealing stage in the MEAUS process is to produce structural changes within the precursor film as a function of annealing temperature, time and tension level. In Fig. 6.2 it is recognized that the 1 st order SAXS peak shifted to lower values of s as the annealing temperature was increased and thus the long spacing (ℓ) increased relative to the precursor. These long spacing results suggest that the average lamellar thickness increased upon annealing relative to the precursor. It is further observed in this figure, that the peak width at half the maximum (Δw) decreased with annealing. This result regarding Δw indicates that the lamellar distribution has become more uniform upon annealing. Also note that as the specific annealing temperature was increased, the crystalline phase thickened (i.e. s* is smaller than the s* value characterizing the precursor) and was more uniform in thickness (i.e., Δw decreases versus the precursor). The annealing temperature effects just described held for all the resin F films and are plotted as a function of annealing time in Fig. 6.3 for ℓ and in Fig. 6.4 for Δw. Upon examination of these figures, when annealing a resin F film, it is recognized that as the annealing time increased, the lamellar thickness increased while Δw decreased.

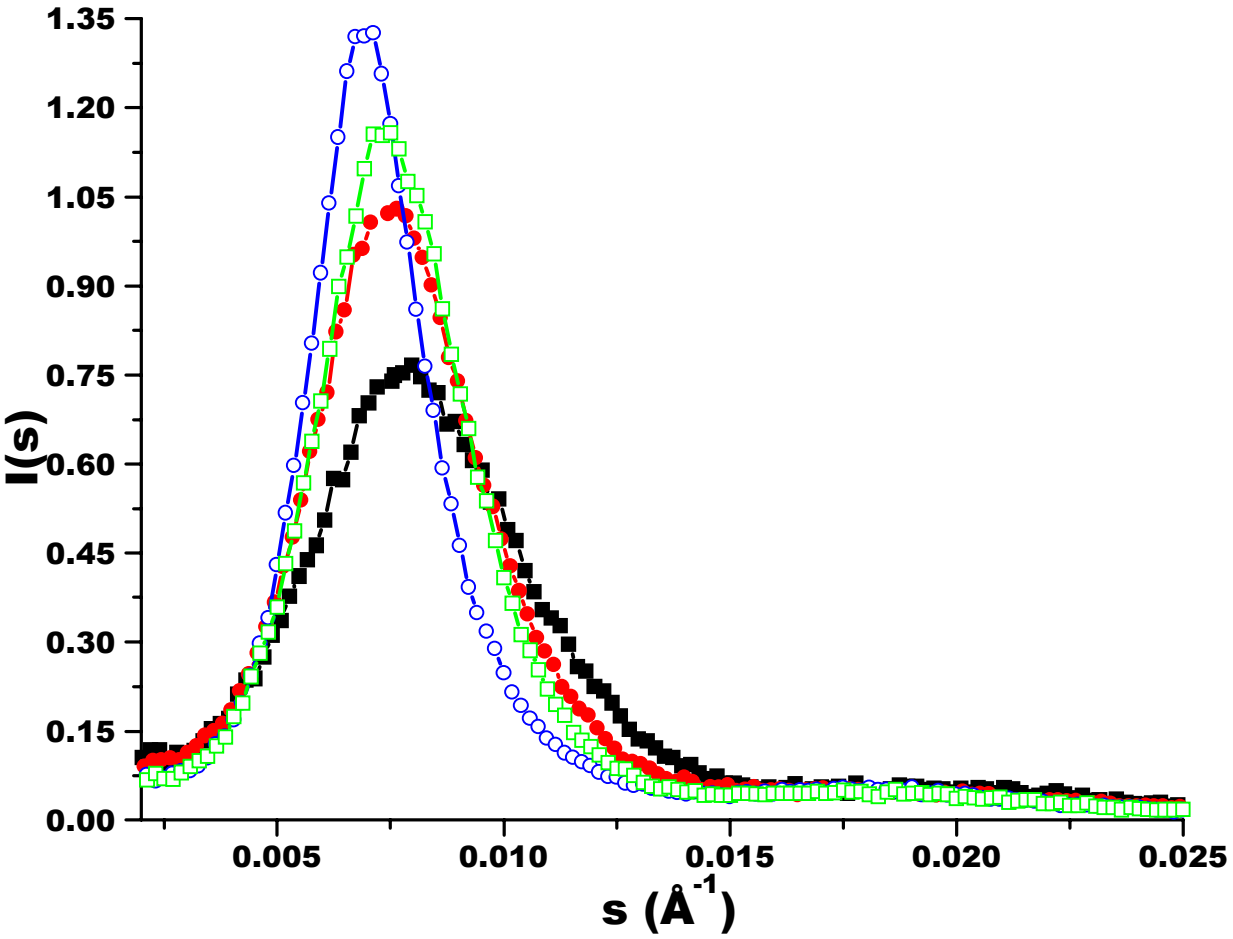

Figure 6.2 Slit-smeared intensity for precursor F1 and F1 free-annealed films as a function of annealing temperature for t_a = 20min: (-■-) precursor, (-●-) T_a = 110°C, (-□-) T_a = 130°C, (-○-) T_a = 145°C.

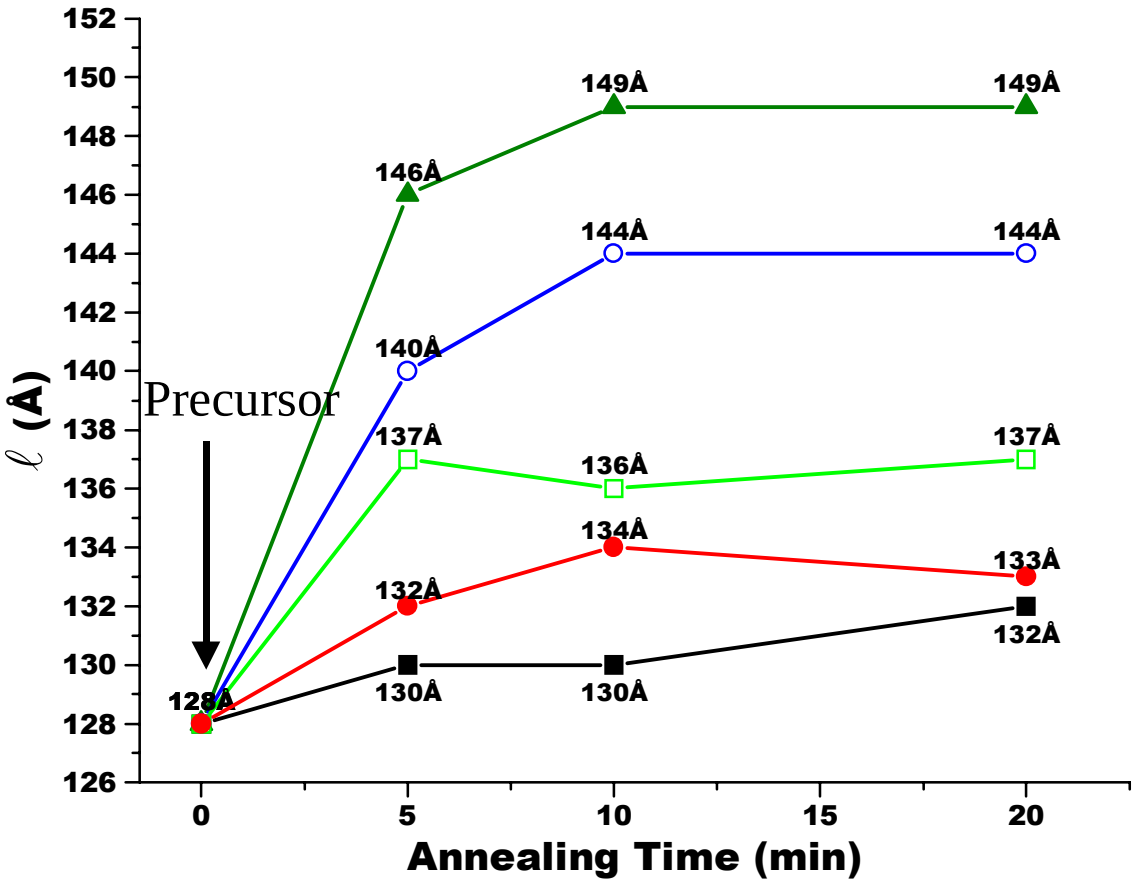

Figure 6.3 Long spacing (ℓ) for free-annealed F1 films as a function of annealing time (x-axis) and temperature: (-■-) T_a = 85°C, (-●-) T_a = 110°C, (-□-) T_a = 130°C, (-○-) T_a = 145°C, and (-▲-) T_a = 150°C.

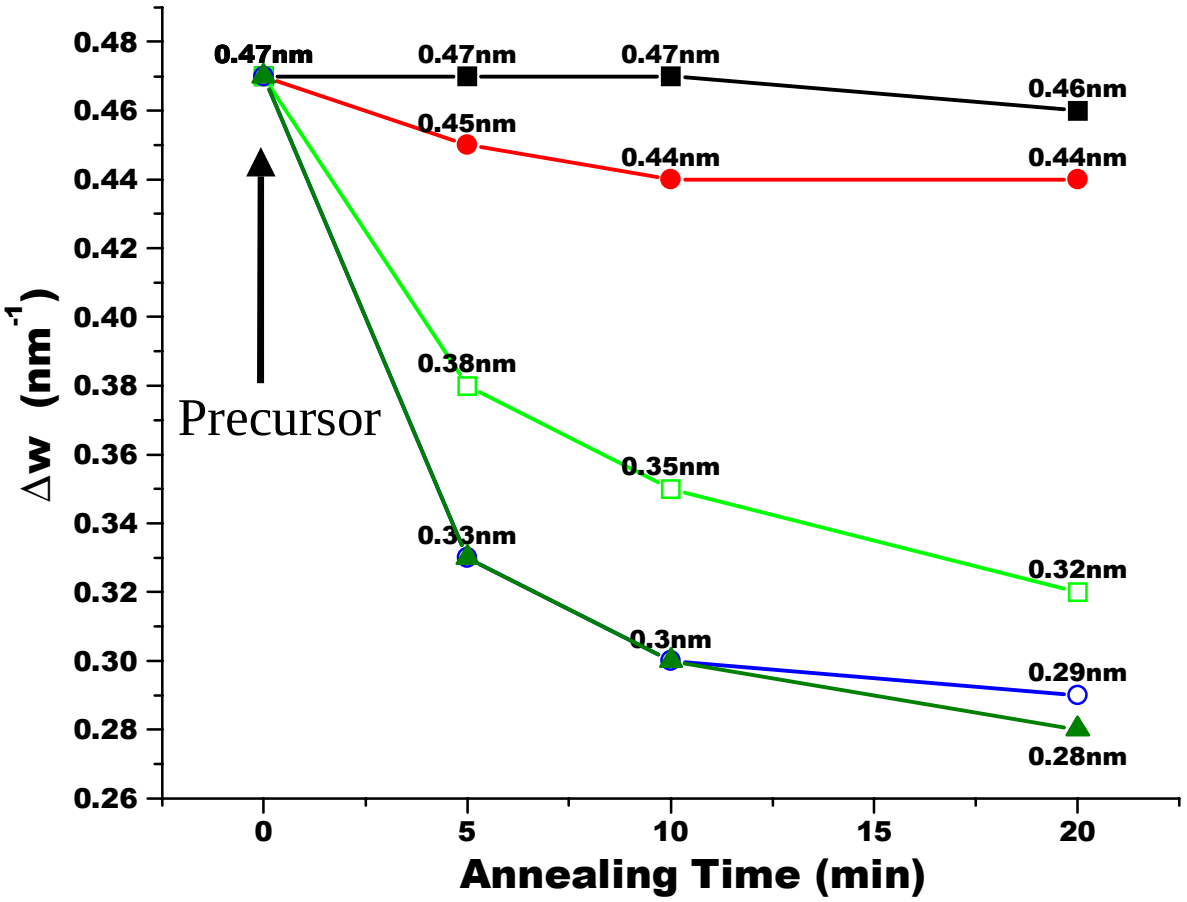

Figure 6.4 Full width at half the maximum of the first order slit-smeared SAXS peak for free-annealed F1 films as a function of annealing time (x-axis) and temperature: (-■-) T_a = 85°C, (-●-) T_a = 110°C, (-□-) T_a = 130°C, (-○-) T_a = 145°C, and (-▲-) T_a = 150°C.

Figure 6.5 presents the slit-smeared SAXS profiles of four D1 free-annealed films with different annealing temperatures (t_a = 20min) and the corresponding precursor. In this figure, it is clear that for the annealing temperatures utilized, lamellar thickening occurred upon annealing the precursor D1. These annealed D1 film results are also tabulated in Table 6.3. It is recognized that the magnitude of the calculated long spacing values for the D1 free-annealed films are much larger than those of the F1 free-annealed films for equal conditions. For example, the D1 film free-annealed at 145°C for 20min was found to possess a long spacing of 181Å while the comparably annealed F1 film was characterized by a value of only 144Å. It is reiterated again that resin F contains ethylene oxide as a comonomer while resin D contains no comonomer.

Table 6.3 Pertinent film characteristics of selected D1 annealed films.

T_a (°C)	precursor	85	120	145	155	160
t_a (min)	-	20	20	20	20	20
% tension	-	free	free	free	free	free
ℓ (Å)	153	155	162	181	200	208
Δw (nm^{-1})	0.49	0.43	0.39	0.30	0.25	0.21

The effect of annealing temperature on the melting endotherm of resin F free-annealed films is displayed in Fig. 6.6. It is observed that the DSC trace was not significantly affected by annealing the film at 110°C relative to the trace of the precursor. However, the F1 films annealed at either 145 or 150°C are characterized by sharper melting profiles shifted to slightly higher temperatures relative to the precursor. Figure 6.7 shows the dependence of T_m and X_c on annealing temperature and time for the F1 free-annealed films. It is found that T_m is *not* systematically shifted to higher temperatures for either annealing temperature (110 or 145°C). In contrast, as annealing time and/or temperature increased, so did X_c for these F1 free-annealed specimens, albeit marginally at the lower temperature of 110°C. These findings along with other pertinent annealing results are displayed in Table 6.4 for the F1 films. While not shown, the D1 films when annealed responded similarly, i.e., X_c was systematically affected by annealing temperature and/or time while T_m was not.

Table 6.4 Pertinent annealed F1 film properties at different t_a (min), T_a (°C), and percent tension combinations.

T_a (°C)	t_a (min)	% tension	T_m (°C)	X_c (%)	f_c
110	5	free	166	48	~0.81
110	20	free	165	50	~0.81
110	20	3%	167	50	~0.81
110	20	15%	166	50	0.76
130	5	free	166	48	~0.81
130	20	free	165	50	~0.81
145	5	free	166	49	~0.81
145	20	free	166	51	~0.81
145	20	3%	168	51	0.80
145	20	9%	167	51	0.75
145	20	15%	166	51	0.69
150	5	free	166	50	~0.81
150	20	free	167	52	~0.81

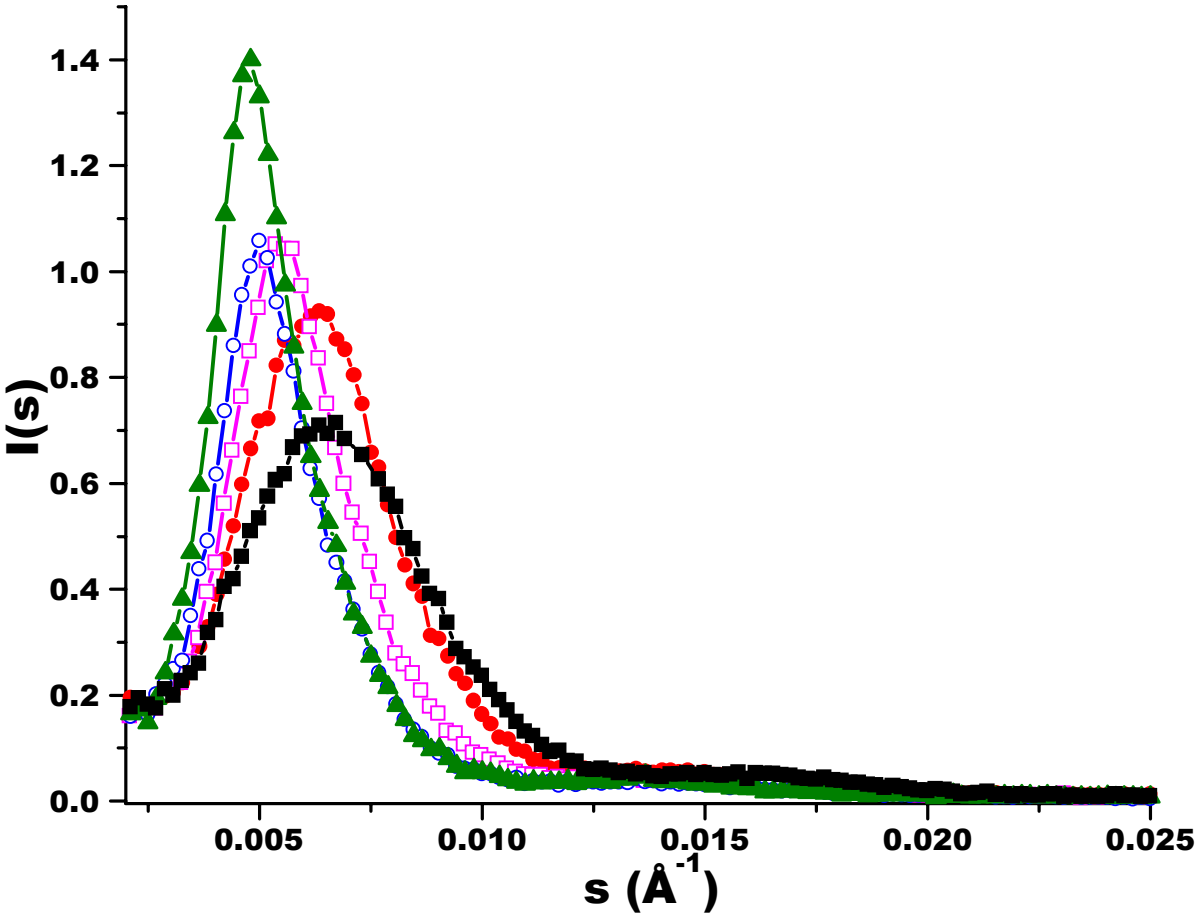

Figure 6.5 Slit-smeared intensity for precursor D1 and D1 free-annealed films as a function of annealing temperature for t_a = 20min: (-■-) precursor, (-●-) T_a = 120°C, (-□-) T_a = 145°C, (-○-) T_a = 155°C, and (-▲-) T_a = 160°C.

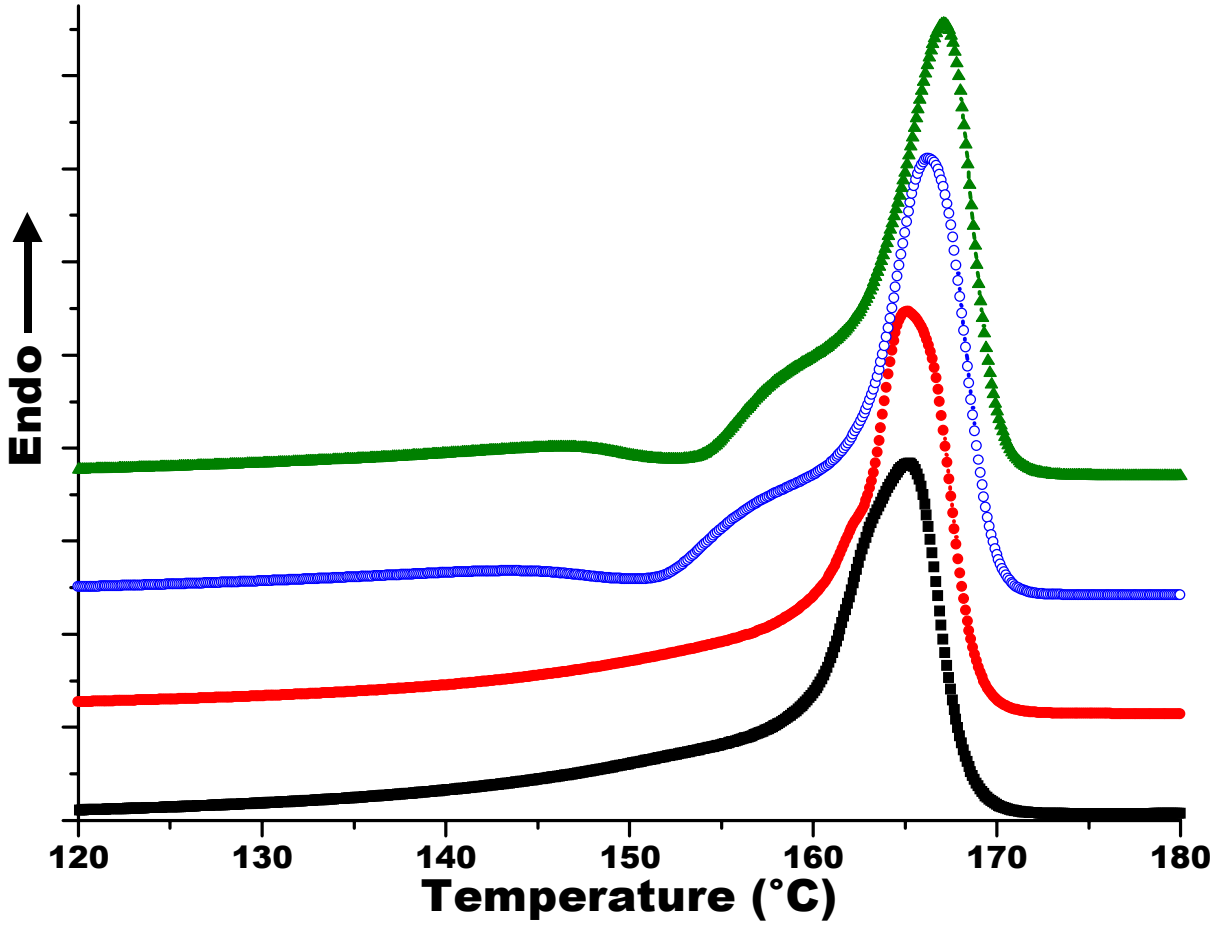

Figure 6.6 DSC heating scans of theF1 precursor and F1 free-annealed films for t_a=20min: (-■-) precursor, (-●-) T_a = 110°C, (-○-) T_a = 145°C, and (-▲-) T_a = 150°C utilizing a heating rate of 30°C/min.

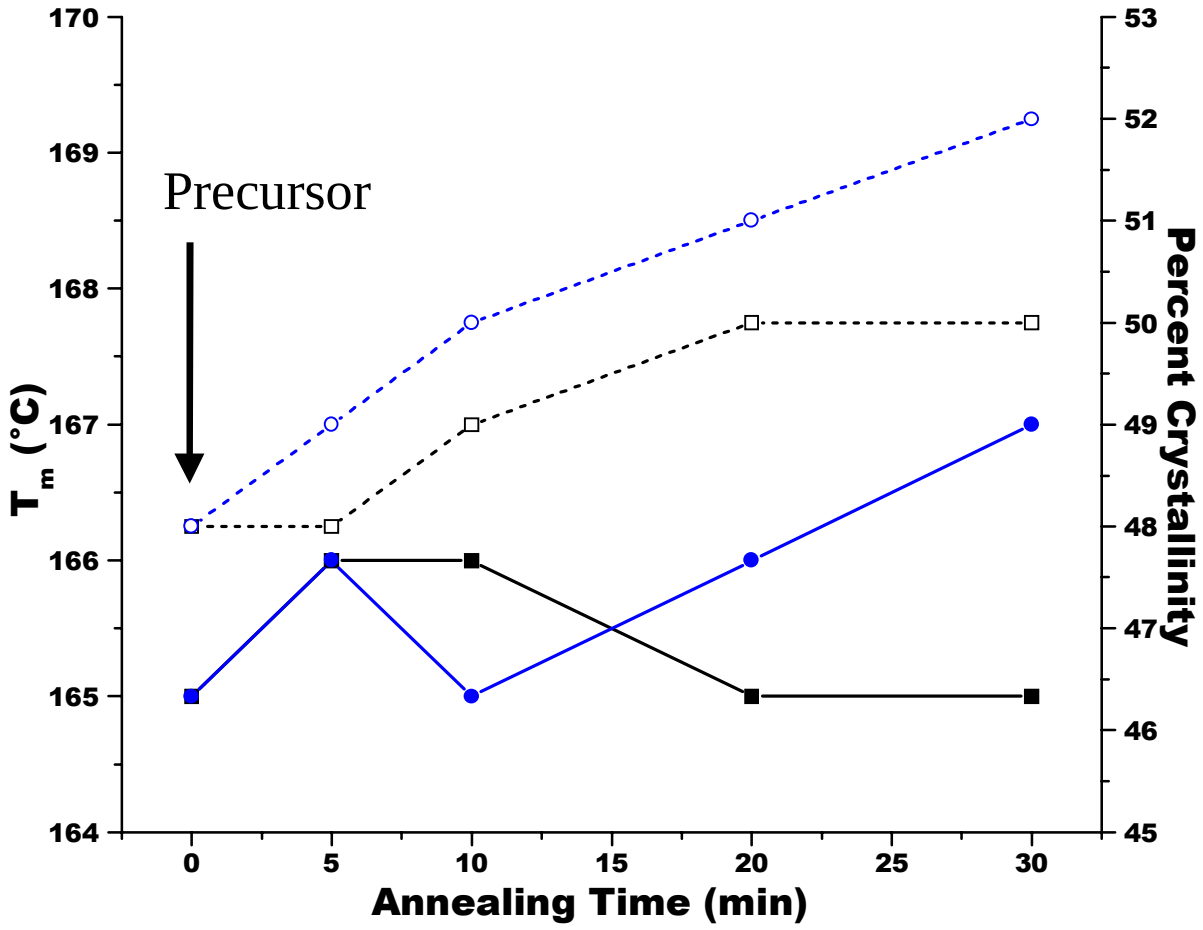

Figure 6.7 The T_m (solid lines & solid data points) and X_c (dashed lines & open data points) results for the F1 precursor and selected F1 free-annealed films as a function of t_a : (-■-) and (-□-) T_a = 110°C; (-●-) and (-○-) T_a = 145°C.

Figures 6.8a and b display the effect annealing temperature (110 or 145°C, respectively) had on the morphology of free-annealed F1 films. It is evident there are not any noticeable differences between these micrographs. In Figs. 6.9a-d, AFM micrographs are presented of F1 annealed films where tension was applied during annealing at a temperature of 110 or 145°C. At lower levels (3%), regardless of annealing temperature (Figs. 6.9a & b), tension does not visibly alter the morphology. However, lamellar deformation is observed for F1 films annealed under higher tension levels (15%) at 145 and 110°C for 20min (Figs. 6.9c & d, respectively). The structural changes displayed in these latter two figures are different from each other. Specifically, for the sample annealed at 145°C, Fig. 6.9c, the lamellae appear to be oriented at an angle to the MD or draw direction. In Fig. 6.9d, void containing morphologies, indicated by arrows, are apparent in this film annealed at a lower temperature (110°C). The presence of voids for the sample presented in Fig. 6.9d, promoted greater turbidity (haze) than the samples in Figs. 6.8, 6.9a-c. In fact, given a specific annealing temperature, the film annealed with the greater level of tension visually displayed a greater level of turbidity. Additionally, for a tension level greater than 3 percent, the sample annealed at a lower temperature visually possessed a greater haze than the film annealed at a higher temperature. Although not presented here, these optical results were independent of annealing time for the processing window studied. An increased turbidity is accounted for by an increase in void content since the voids induced by tension increase the number of interfaces within the film, and as a result a greater fraction of the incident light is scattered and/or reflected. The development of voids with increasing tension is also supported by the slit-smeared SAXS data, as displayed in Figs. 6.10a and b, for a number of the same films presented in Figs. 6.8 & 6.9. In the case of Fig. 10a, the SAXS profiles are provided for each sample annealed at a lower tension level (≤ 3%). Each profile displays a first order scattering peak with a value of s* consistent with those determined for the comparably free-annealed specimens. In other words, the long spacing values obtained for the annealed samples, when the tension was lower (≤ 3%), were only dependent upon the temperature or time of annealing. Further, the sample annealed at the higher temperature (145°C) under 15 percent tension is characterized by a value of s* similar to the sample annealed at the same temperature but a lower tension level (i.e. T_a = 145 at 3% tension). The scattering profiles of these two films differ only in the peak intensity (I(s)), where the higher the tension level, the lower the value of I(s). In Fig. 6.10b, the SAXS profiles of samples annealed at a lower temperature (110°C) but at 15 percent tension for 5 or 20min are provided. It is noted that the samples presented here, possesses an extremely high peak intensity characterized by a much lower value of s*. In fact,

the value of s* is associated with a long spacing equal to approximately 14 nm. This long spacing compares quite closely with the void size (along MD) estimated for a few of the structures observed via AFM in Fig. 6.9d. It is also recognized that this finding is independent of the annealing time used. The authors note that the above SAXS, DSC, and AFM findings as well as the optical observations were found to occur for all resin F films.

The reader will recall from Table 6.4 that there was also an effect of tension during annealing on the crystal "c"-axis orientation (f_c). Specifically, the orientation unexpectedly decreased as the specific tension level utilized increased above 3 percent. For a specific tension level of 3 percent or greater, the orientation also generally decreased as the isothermal annealing temperature increased (e.g. 110 vs. 145°C). Thus, a film annealed at 110°C for 20min under 15 percent tension possessed a lower f_c than a film annealed at 145°C when all other MEAUS variables were held constant. These results imply that the azimuthal dependence of the (100) reflection decreased as the tension level or annealing temperature increased as long as the tension was greater than 3 percent. It is the (100) reflection that is used to calculate f_a and thus f_c as described previously[3]. Although not shown here, the value of f_c was unaffected by annealing time.

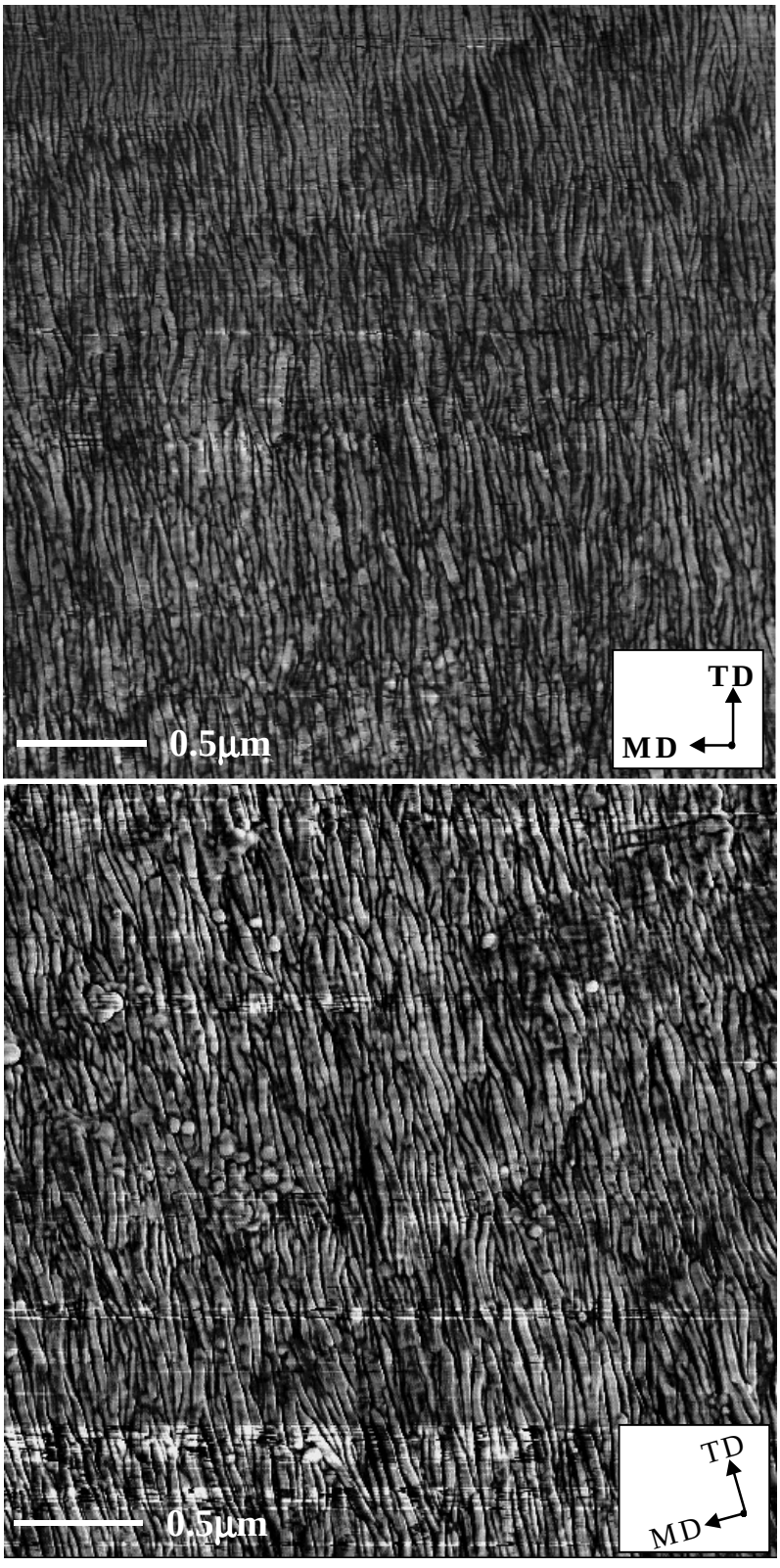

Figure 6.8 AFM images of F1 films free-annealed for 20min a) T_a = 145°C and b) T_a = 110°C. The MD is labeled. Phase images are each 3μm x 3μm.

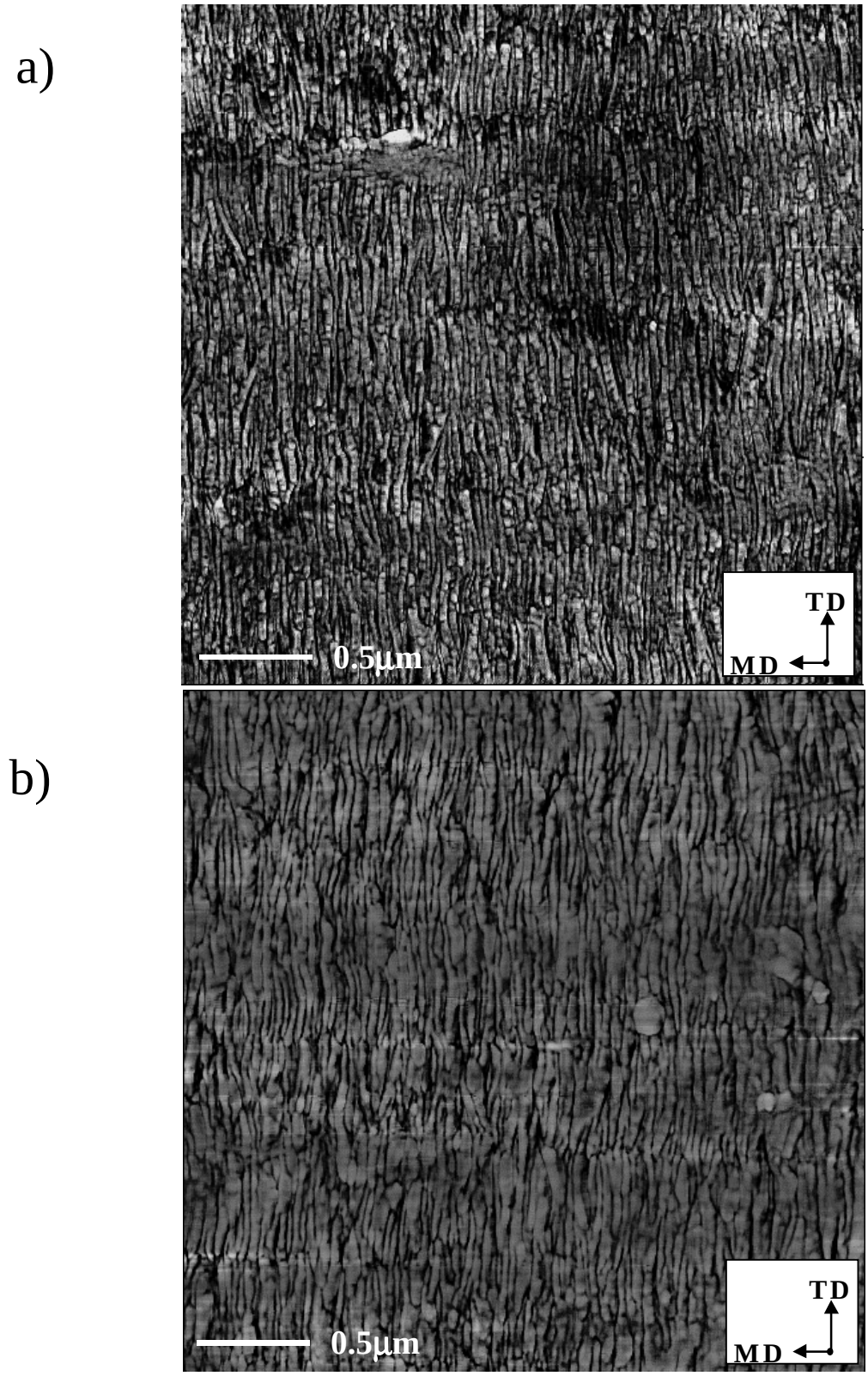

Figure 6.9 AFM phase images of F1 films annealed for 20min under tension a) 3% tension, T_a= 145°C; b) 3%, 110°C; c) 15%, 145°C; and d) 15%, T_a = 110°C;. The MD is labeled. Images are each 3µm x 3µm.

c)

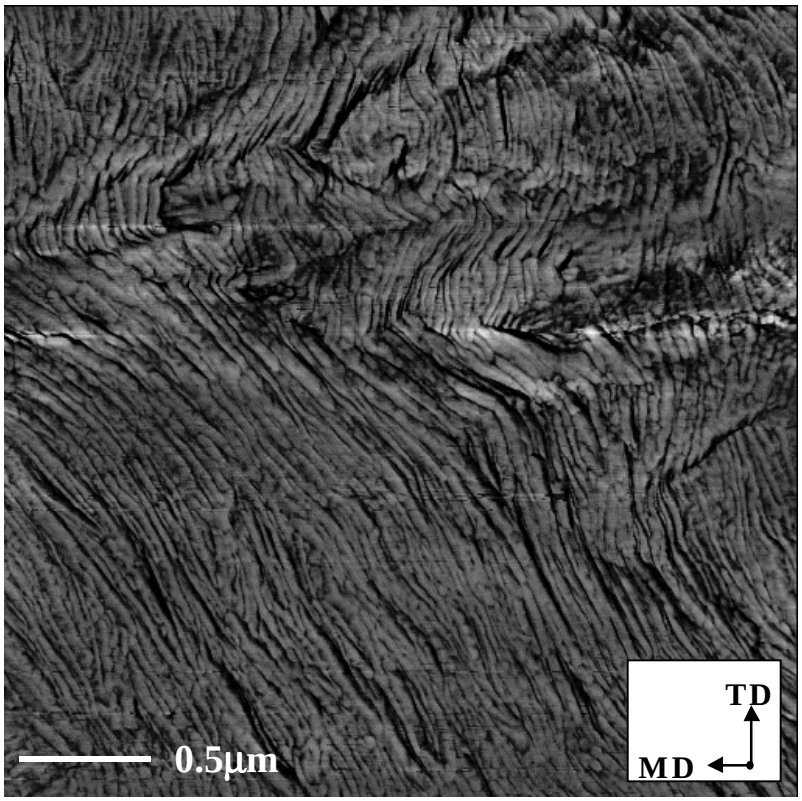

d)

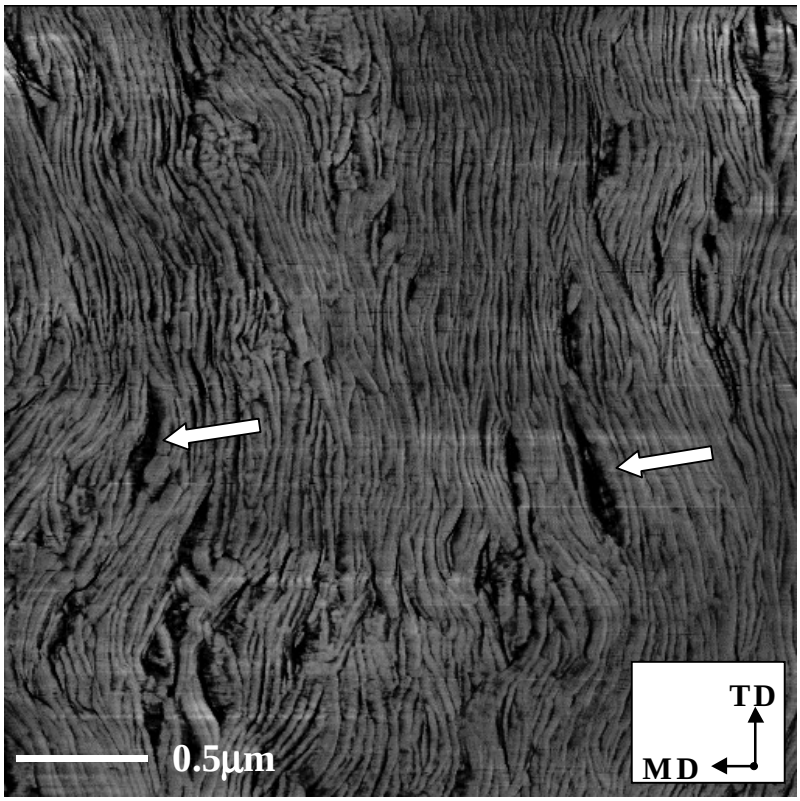

(Figure 6.9 cont'd)

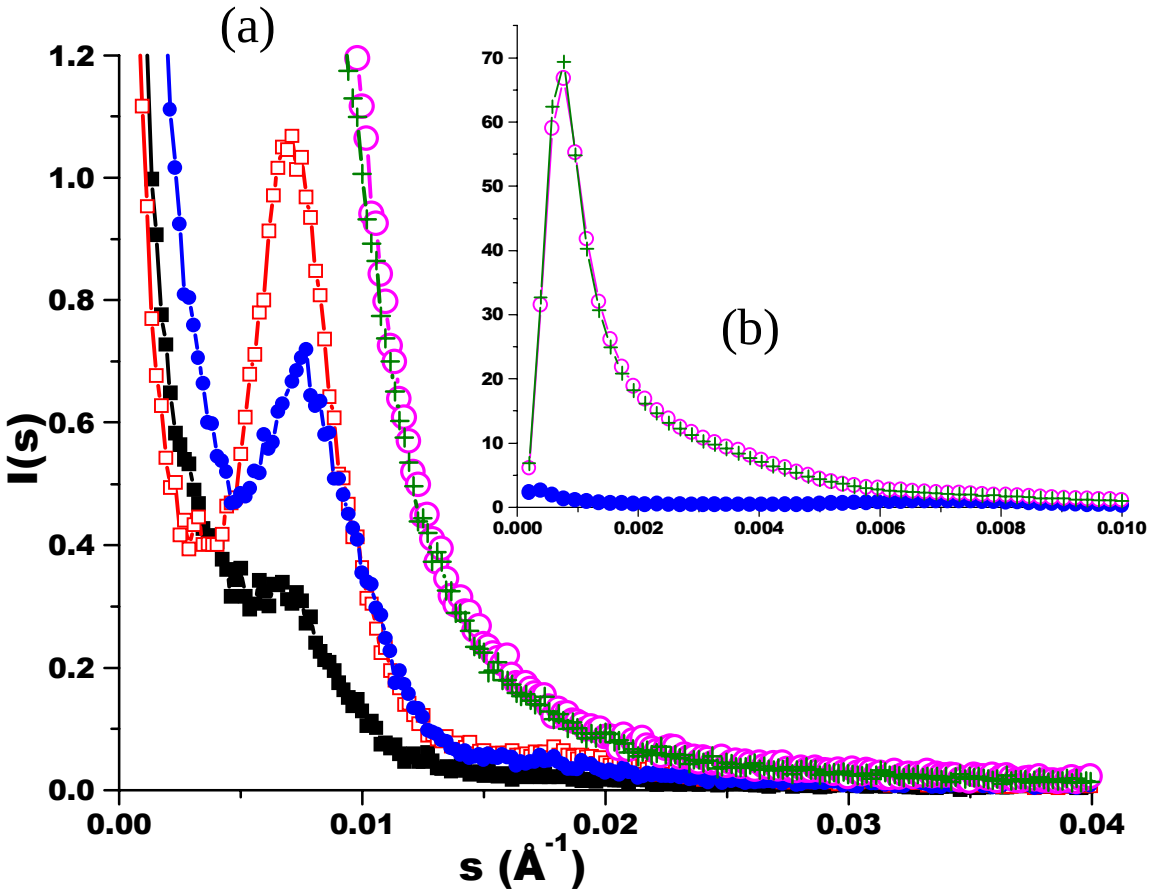

Figure 6.10 Slit-smeared intensity for F1 annealed films under tension: (-■-) T_a = 145°C, t_a = 20min, 15% tension; (-□-) T_a = 145°C, t_a = 20min, 3% tension; (-○-) T_a = 110°C, t_a = 20min, 15% tension; (-+-) T_a = 110°C, t_a = 5min, 15% tension; (-●-) T_a = 110°C, t_a = 20min, 3% tension.

Figure 6.11a-d displays the WAXS patterns obtained for selected F3 annealed films with the X-ray beam along the film ND. These photographs are of annealed films from the precursor F3 where different tension levels (0 or free, 3, 9, and 15%) were applied at a temperature of 145°C for 20min. The f_c values corresponding to the films represented in Fig. 6.11a-d are ca. 0.63, 0.61, 0.55, 0.44, respectively. It is also apparent in these WAXS photographs that the *meridonal* intensity of the (100) reflection, due to some "a"-axis orientation, is observably more intense for the sample annealed at 3 percent tension than for any other presented. As the tension level was further increased to 9 percent, the meridonal reflection disappeared and was totally absent for the sample annealed with 15 percent tension. Although the precursor photograph is not shown here, it was similar to the WAXS pattern for the free-annealed film. These results were independent of annealing time. As previously reported[3], the F1 precursor displayed little "a"-axis orientation, as indicated by its WAXS pattern while the F3 precursor displayed greater "a"-axis orientation along MD and thus is shown. The same trend just described, however, occurred for all resin F films.

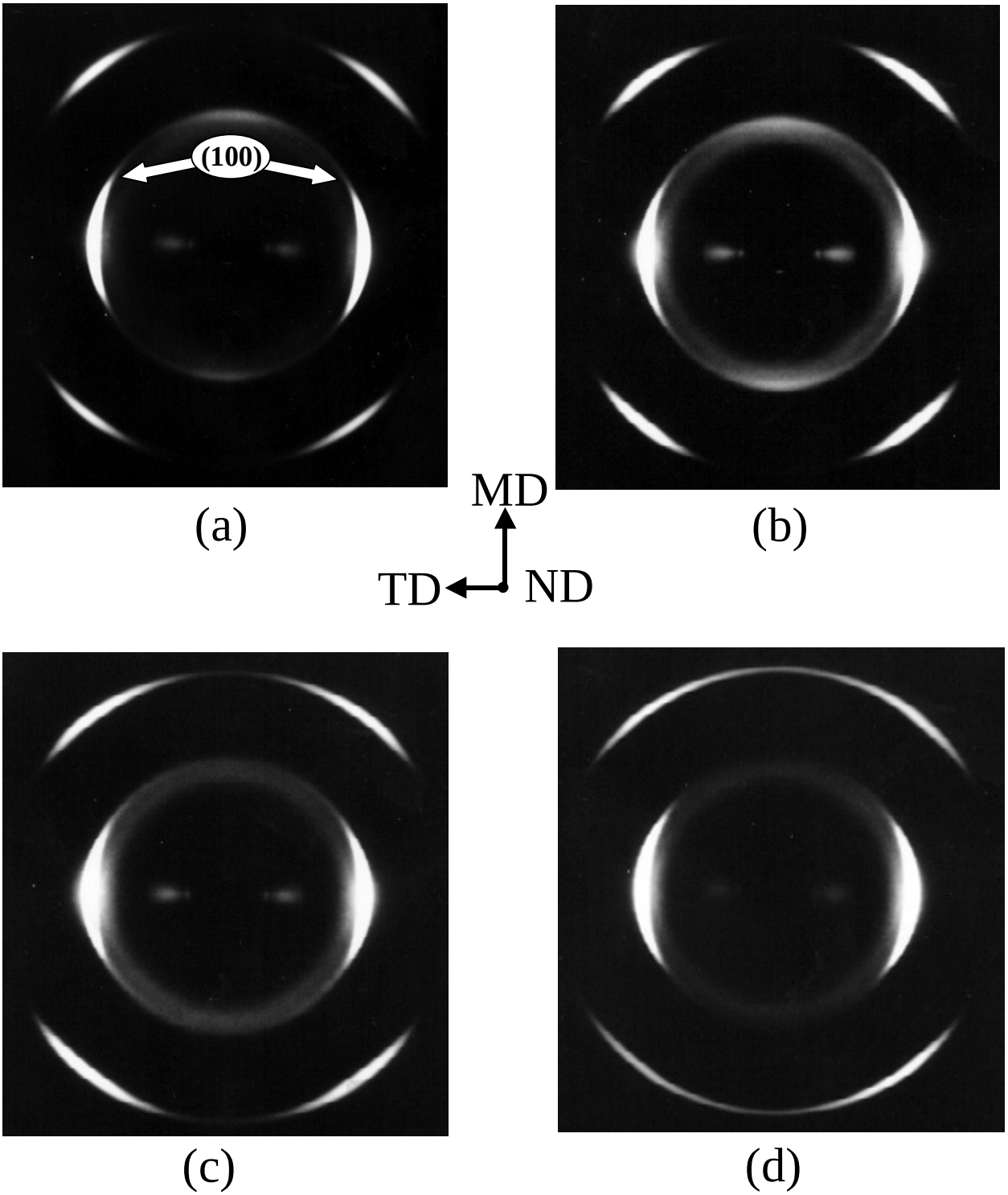

Figure 6.11 WAXS photographs of the F2 annealed films with tension where T_a =145°C for t_a = 20 min: a) free annealed, b) 3% tension, c) 9% tension, and d) 15% tension. The MD is labeled.

6.3-2 Stretching:

The annealed films were subjected to the two step stretching process. Besides crosshead speed, which was kept constant throughout the entire study at 150 mm/min, there were two main variables to be accounted for in each step. The first was temperature (cold stretch and hot stretch temperature), and the second was the percent extension the film was subjected during each step. The cold stretch temperatures studied were 25, 35, 50, and 70°C while the extension levels utilized were 50, 70, and 90 percent. The hot stretching temperatures (T_{hs}) utilized were 85, 100, 115, 130, and 145°C with levels of extension (%HS) of 50, 65, 80, and 90 percent. The levels of extension were calculated using Eqn. 6.3.

$$\%\,\text{Extension} = \frac{l_f - l_o}{l_o} \times 100\% \qquad \text{(Eqn. 6.3)}$$

where l_f is the final length of the film after the cold stretch or hot stretch step and l_o is the initial length of the film *prior to any cold stretching*.

For this investigation, the film was not allowed to relax after stretching, i.e., relaxation will be zero. This is due to the adverse affects relaxation was found to have on film permeability.[2] A heat-setting step was employed for *all* films having undergone the stretching stage. This was done so that the film retains approximately the same dimensions after removal from the stretching device. The heat-setting step occurred immediately after hot stretching in the same oven at the same hot stretch temperature for a period ca. 10 minutes.

From the above, it clear that the possible number of annealing/stretching combinations is large, but the authors do not want to give the impression that every combination was attempted. Instead, the samples reported here will represent the general findings and will be based on a *"standard" set of annealing and stretching conditions*. Any variation(s) from these conditions will be noted. These standard conditions consisted of a film free-annealed at 145°C for 20 min, followed by cold stretching at 50°C to 50 percent extension, then hot stretching at 100°C to an extension level of 90 percent. Heat setting occurred at the hot stretching temperature for 10 min. When any variation was made to this standard stretching condition, the remaining parameters were *not* altered, unless otherwise noted. Thus, a simple sample nomenclature was developed to track the sample history in this annealing/stretching report. This nomenclature designates the final film based upon its precursor and the particular variable(s) that was altered. For example, if a F1 film was annealed at 85°C instead of 145°C, following stretching, the final sample would be labeled F1-T_a85. The remaining annealing and stretching conditions would be analogous to the standard conditions given above.

The effects of annealing on the structure and morphology are addressed first regarding their influence on microporosity after stretching. The Gurley number dependence on annealing temperature is shown in Fig. 6.12 for stretched films from the precursors F1 and F2. The Gurley number, inversely related to permeability and porosity, was found within error to decrease as the isothermal annealing temperature increased to 145°C where the lowest Gurley value was obtained. However, this measure of film permeability increased as the annealing temperature was increased to 150°C. This trend occurred for both sample series F1 and F2 with the F1 membranes possessing higher permeability than the F2 counterparts. The reader may recall that the F1 precursor possessed a higher f_c than did the F2 precursor. A suitable or "quality" porous membrane is defined here as one possessing a Gurley number of 100 seconds or less. Within error, all the F1 final film results in Fig. 6.12 suggest "quality" membranes, but there are not any "quality" Gurley numbers for the F2 samples presented in this figure.

Figures 6.13a-d presents the morphologies, as obtained via AFM, corresponding to some of the results within Fig. 6.12. Figures 6.13b and d each display an image of the F1 film prepared using the standard condition. The latter of these is of a higher magnification image for better observation of a the membrane's finer structure. Figure 6.13a, which is of film F1-Ta110C, possesses less numerous and smaller micropores than the other two films annealed at higher temperatures. The authors have noted that most POM microporous membranes have an appearance that is somewhat different than those of the HDPE[12], isotactic polypropylene[13], or PMP[2] polyolefin films known to produce micropores. Specifically, the lamellae individually splay apart in the POM membranes while the polyolefin films tend to possess many lamellar bundles or "islands" between micropores. Additionally, the micropores are not as large in the POM final films as those in the polyolefin stretched samples. It is, however, recognized that both polyolefin and POM microporous membranes are characterized by bundles of tie-chains between lamellae oriented parallel to the stretch direction (MD).

Annealing time also influenced microporosity as measured via Gurley number with supporting data given in Fig. 6.14. In this figure, the Gurley value results are a function of annealing time for stretched films from precursors F1 and F2. As the annealing time was increased, the film permeability increased. Again, the F1 stretched films are characterized by higher porosity than the F2 materials for equal conditions.

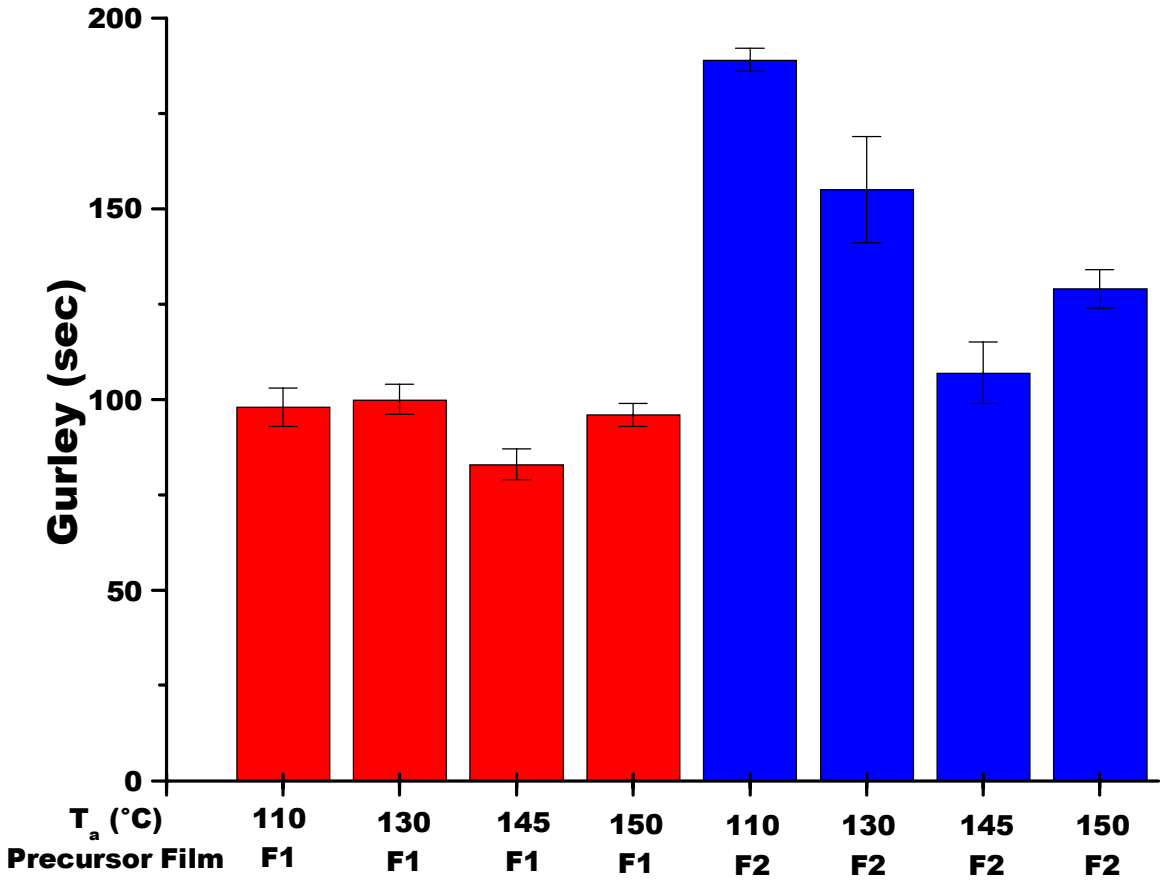

Figure 6.12 Effect of annealing temperature on the Gurley number for F1 and F2 stretched films. The other annealing/stretching parameters remained constant with the standard condition.

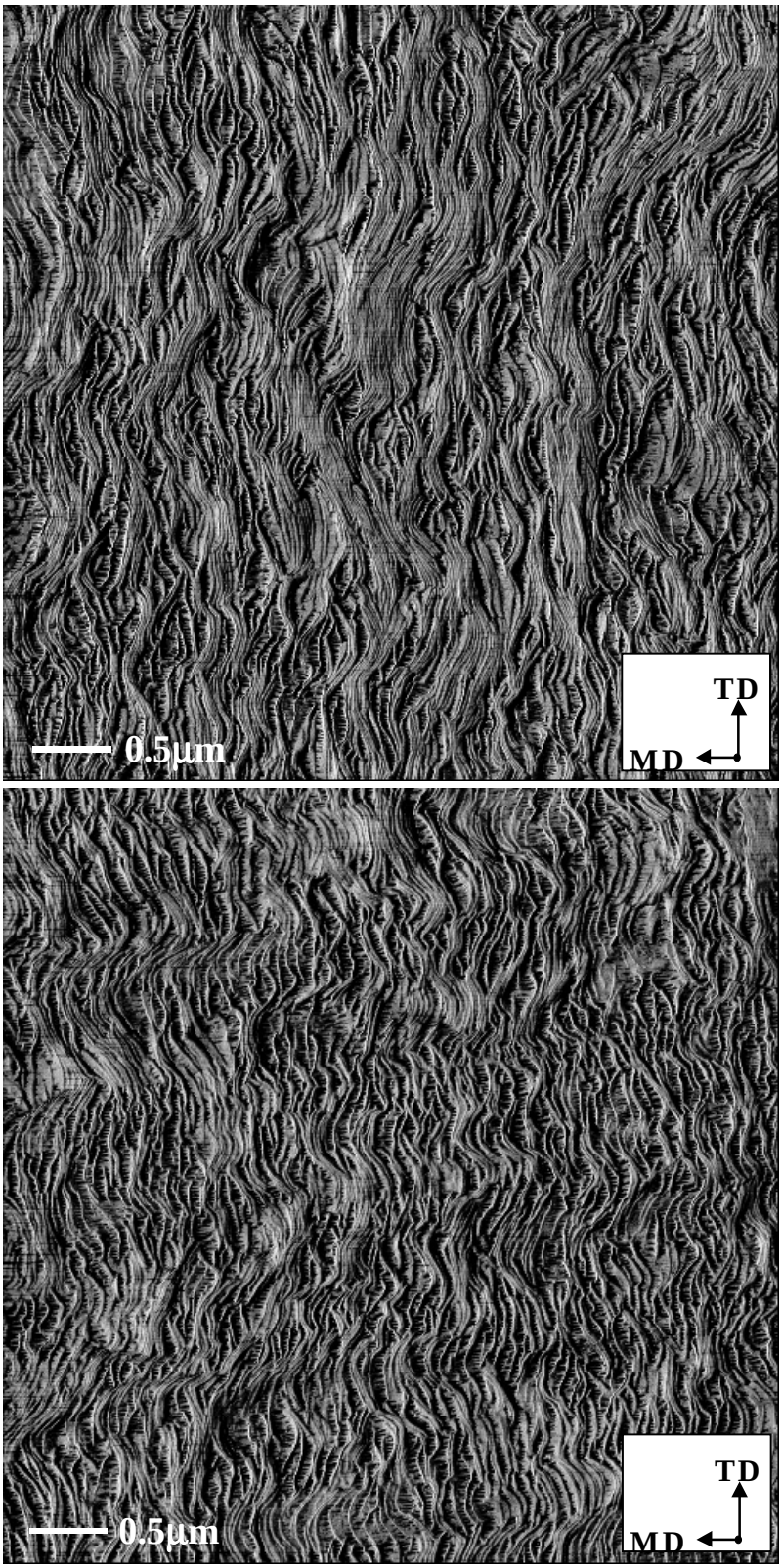

Figure 6.13 AFM phase images of the resin F POM stretched films a) F1-T_a110C, b) F1-T_a145C (standard condition), c) F1-T_a150C, and d) 2µm x2µm image of b). The MD is labeled. Images are each 5µm x 5µm except for fig d).

c)

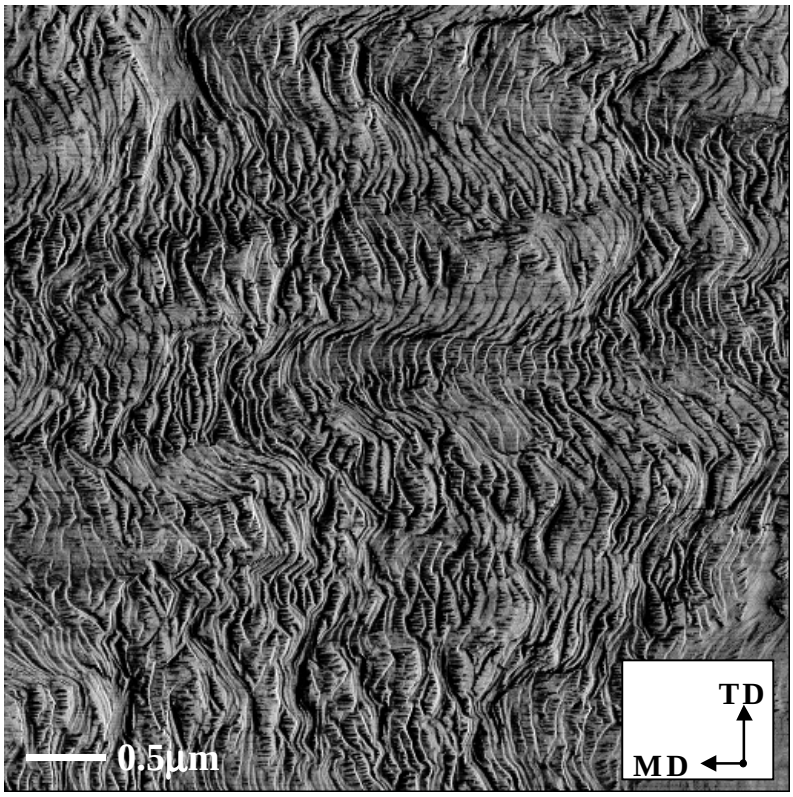

d)

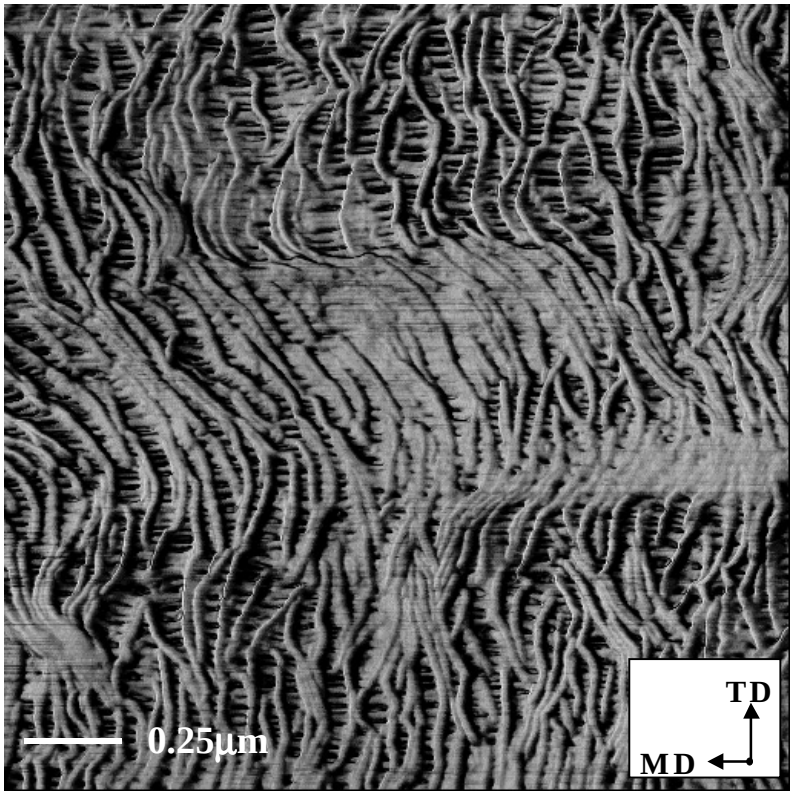

(Figure 6.13 cont'd)

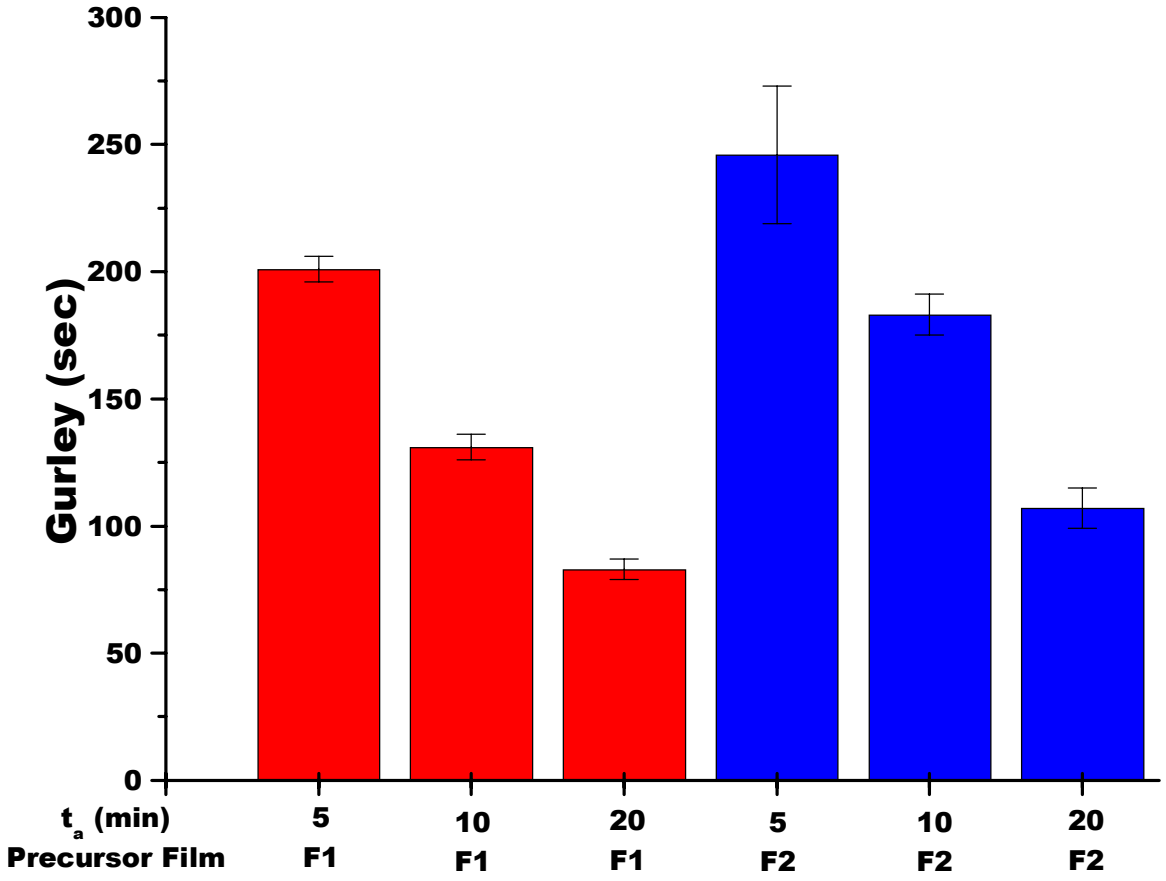

Figure 6.14 Effect of annealing time on the Gurley number for F1 and F2 stretched films. The other annealing/stretching parameters remained constant with the standar d condition.

The application of tension during annealing was shown earlier in this report to alter the annealed film morphology and thus it was expected to impact the microporous structure and permeability of the final film. Data supporting this statement is given in Fig. 6.15 for both F1 and F2 films. In either film series, higher tension levels (percent extension) during annealing yield higher Gurley numbers following stretching. In fact, films annealed with 15 percent tension possessed non-porous properties as indicated by a Gurley value greater than 1000 seconds. This result was regardless of the resin F precursor used. However, some "quality" membranes were obtained from both film series. The effect of tension during annealing on the stretched film microporous structure for films F1-3%tension and F1-9%tension is shown via AFM in Figs. 6.16a & b, respectively. For comparison, these micrographs should be contrasted against a membrane produced using the standard condition - recall Fig. 6.13d. Clearly, the microporous character was eliminated as the tension level increased. These morphological results are somewhat expected based upon the Gurley numbers previously discussed. In summary of the annealing effects, the Gurley value, the stretched film thickness, and the normalized Gurley number to film thickness values are presented in Table 6.5 for a number of F1 membranes. The Gurley numbers normalized on film thickness, which are more accurate values for membrane comparison, verify the trends regarding the influence of the annealing conditions on the stretched films discussed above.

Table 6.5 Pertinent annealed F1 film properties at different t_a (min), T_a (°C), and percent tension combinations, where all other annealing/stretching parameters remained constant with the standard condition.

T_a (°C)	t_a (min)	tension (% Exten.)	Gurley (sec)	Film Thickness (mil)	Norm. Gurley (sec/mil)
110	20	free	98 ± 5	0.76	129
110	20	3%	215 ± 21	0.74	290
110	20	15%	≥ 1000	-	-
130	5	free	223 ± 22	0.76	293
130	20	free	100 ± 4	0.76	132
145	5	free	201 ± 5	0.75	268
145	20	free	83 ± 4	0.78	106
145	20	3%	131 ± 11	0.76	172
145	20	9%	651 ± 233	0.73	892
145	20	15%	≥ 1000	-	-
150	5	free	125 ± 15	0.75	167
150	20	free	96 ± 3	0.73	132

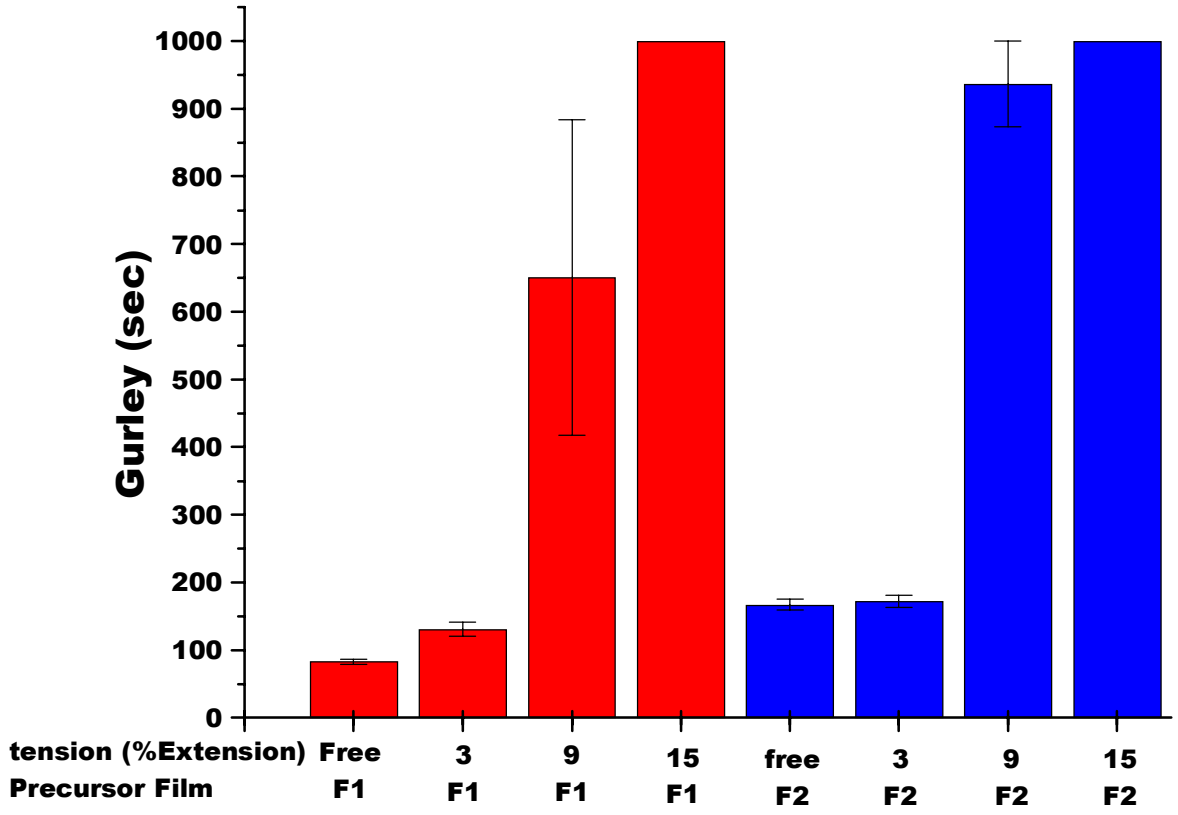

Figure 6.15 Effect of tension level during annealing on the Gurley number for F1 and F2 stretched films. The other annealing/stretching parameters remained constant with the standard condition.

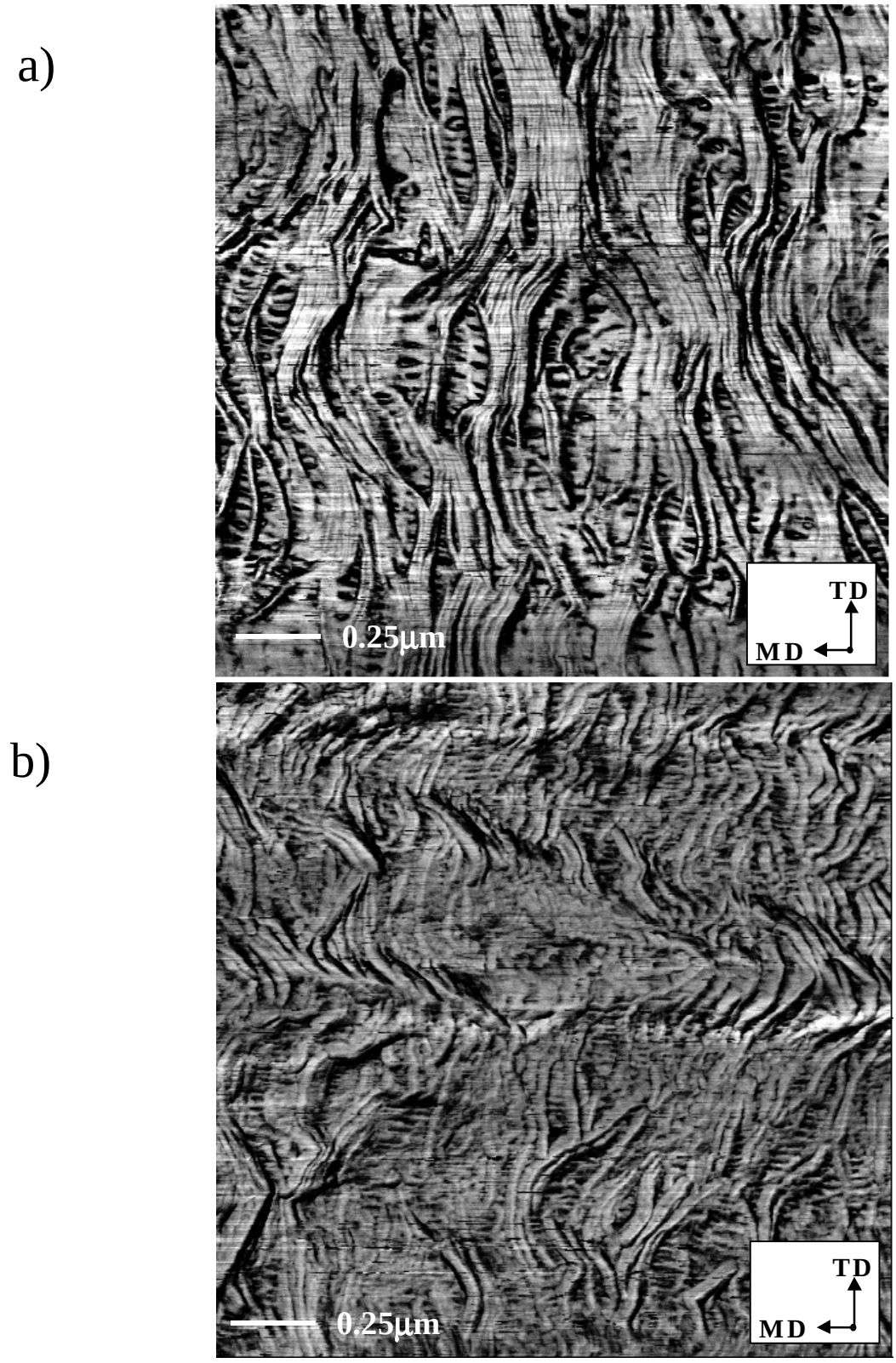

Figure 6.16 AFM images of the resin F POM stretched films displaying the effect of tension during annealing on the microporosity: a) 3% tension and b) 9% tension. The MD is labeled. The images are each 2μm x 2μm.

We now address the uniaxial-stretching stage of the MEAUS process with the presentation of the cold-stretching results. Since it has been established that the permeability (as related to Gurley) of the F2 films parallel the trends of F1 membranes, only the stretching results from the precursor F1 will be given. Figure 6.17 is a plot of the Gurley values as a function of both the percent cold stretch extension (x-axis) and stretching temperature for F1 membranes. It is apparent that as the extension was increased, the Gurley number decreased. The lowest Gurley value occurred for the film cold stretched to 90 percent at a temperature of 50°C. Membranes produced using this cold stretch temperature (50°C) possessed the highest porosity followed by those final films cold stretched at temperatures of 70 and 35°C, respectively, for comparable annealing and stretching conditions. These Gurley values along with others that resulted from different cold stretch variable combinations are presented in Table 6.6. The trends described above still existed for the normalized results although this data is not presented here.

Table 6.6 The Gurley number results from membranes of different %CS and T_{cs} combinations. All other annealing/stretching parameters remained constant with the standard condition.

T_{cs} (°C) \ %CS (%Extension)	50	70	90
25	423 ± 24 sec	NP	NA
35	206 ± 22 sec	172 ± 11 sec	139 ± 9 sec
50	83 ± 4 sec	76 ± 3 sec	63 ± 3 sec
70	133 ± 2 sec	98 ± 6 sec	82 ± 4 sec

*NP denotes a sample that was not produced because sample rupture occurred repeatedly for a number of attempts during cold stretching.
**NA denotes a variable combination that was not attempted.

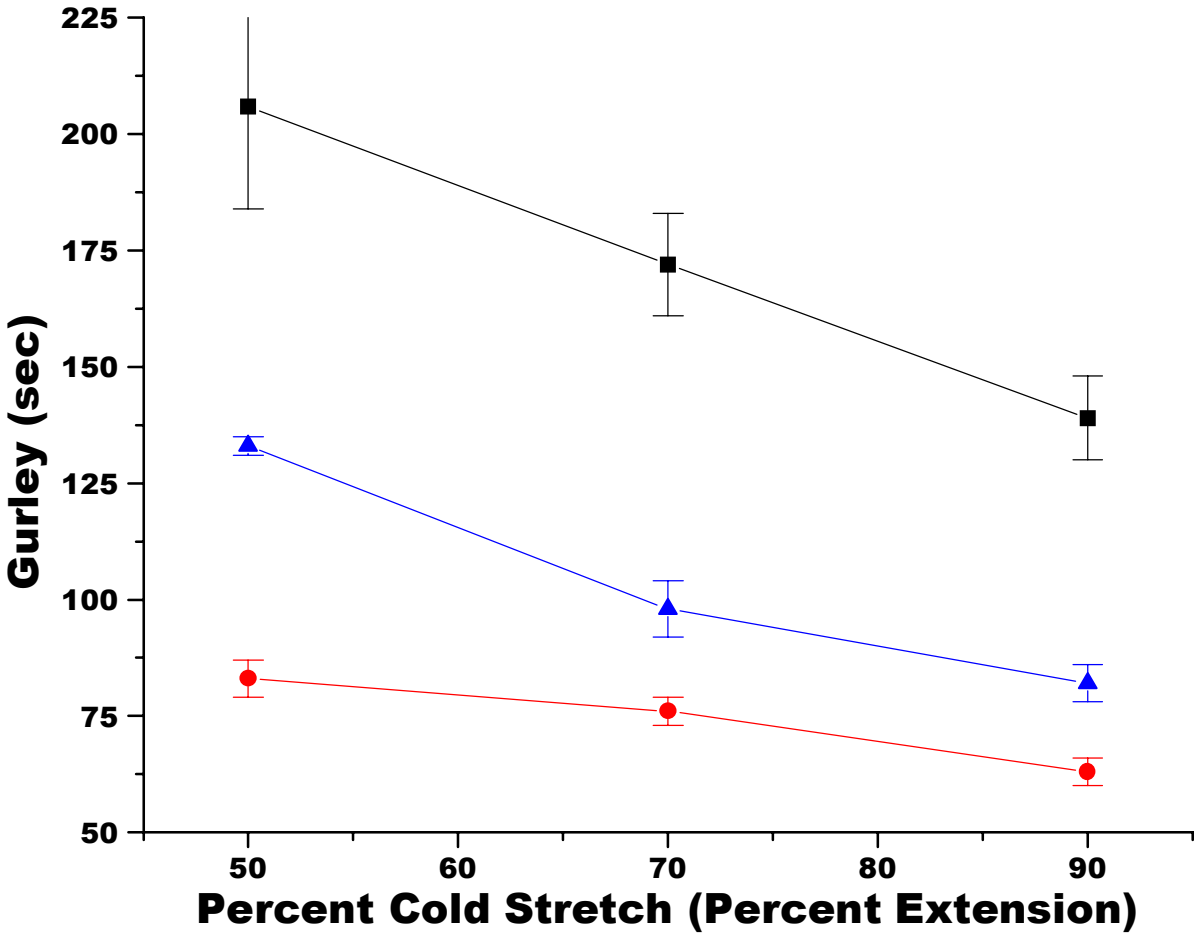

Figure 6.17 Effect of the cold stretch parameters (T_{cs} and %CS) on the Gurley number for F1 stretched films (-■-) T_{ca} = 35°C, (-●-) T_{ca} = 50°C, and (-▲-) T_{ca} = 70°C. The other annealing/stretching parameters remained constant with the standard condition.

The influence of the hot stretching parameters on membrane permeability is shown in Fig. 6.18. Table 6.7 presents the membrane Gurley values that are a result of a number of additional hot stretch variable combinations with the remainder of the standard conditions intact. The figure displays the expected results concerning the percent hot stretch and its influence on permeability; as the percent hot stretch extension increases, so does permeability. It was also found that the temperature at which hot stretching occurs affected the Gurley values in the following manner. As the temperature was increased from 85 to 100°C, permeability increased; however, further increasing the temperature above 100°C produced a decrease in permeability. In fact, at a hot stretch temperature of 145°C, which is equal to the standard annealing temperature, the films were impermeable. This is especially apparent upon observing the morphology of this film as shown in Fig. 6.19. This lack of porosity occurred for any membrane that was hot stretched at a temperature equal to or greater than its annealing temperature (i.e. $T_{hs} \geq T_a$). Although the normalized Gurley values are not presented here, the data trends just described were not different.

Table 6.7 The Gurley number results from membranes of different %HS and T_{hs} combinations. All other annealing/stretching parameters remained constant with the standard condition.

T_{hs} (°C) \ %HS (%Extension)	50	65	80	90
85	357± 5 sec	271 ± 21 sec	113 ± 4 sec	98 ± 15 sec
100	113 ± 12 sec	92 ± 2 sec	84 ± 6 sec	83 ± 4 sec
115	132 ± 15 sec	112 ± 11 sec	95 ± 5 sec	86 ± 5 sec
130	541 ± 91 sec	478 ± 83 sec	394 ± 43 sec	345 ± 20 sec
145	≥ 1000 sec	≥ 1000 sec	≥ 1000 sec	≥ 1000 sec

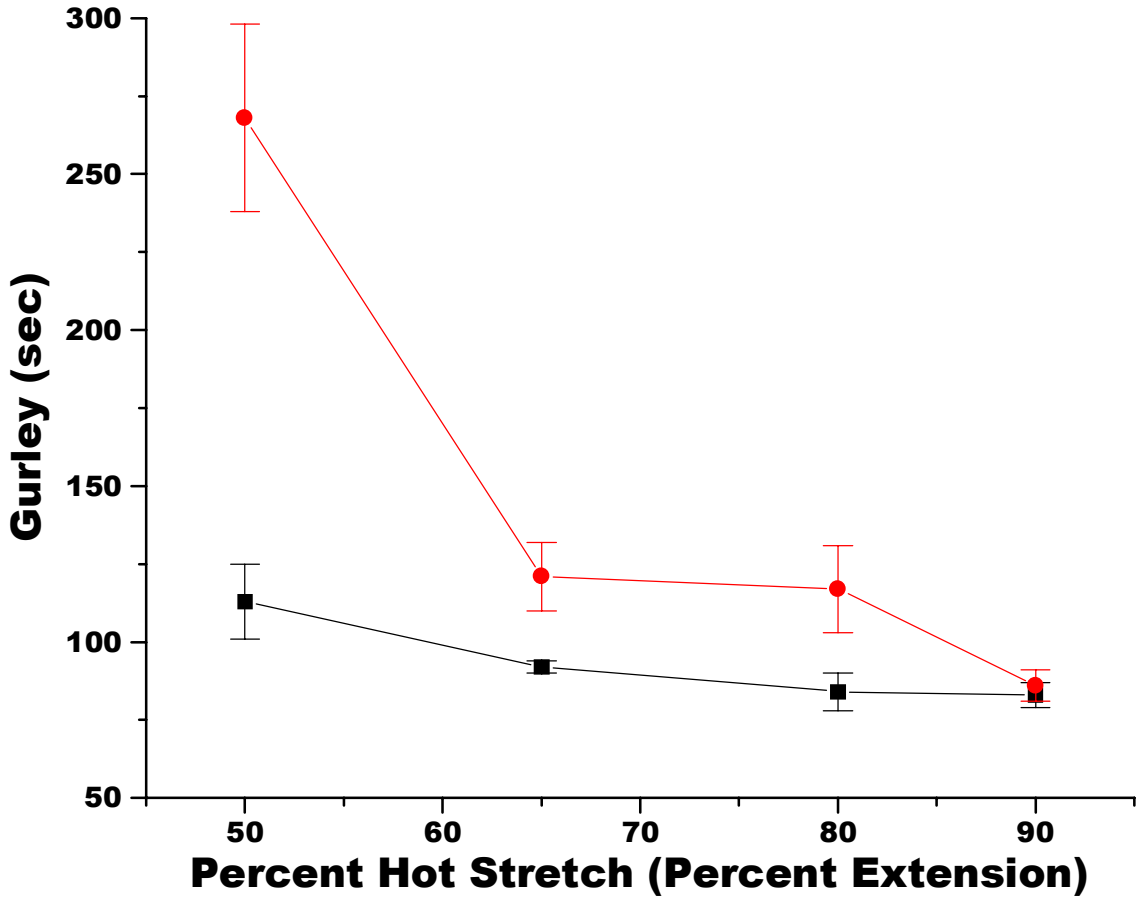

Figure 6.18 Effect of the hot stretch parameters (T_{hs} and %HS) on the Gurley number for F1 stretched films (-■-) T_{hs} = 100°C and (-●-) T_{hs} = 115°C. The other annealing/stretching parameters remained constant with the standard condition.

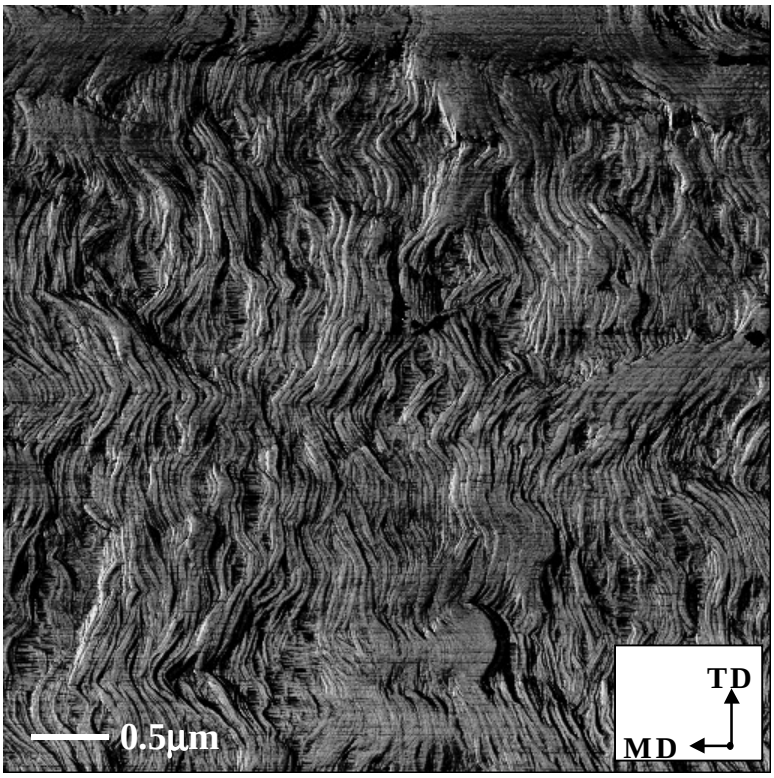

Figure 6.19 AFM phase image of the F1 stretched film F1-T_a110C,T_{hs}145C displaying the effect on microporosity when $T_{hs} > T_a$. The MD is labeled, and the image is 5µm x 5µm.

If the Gurley value is plotted as a function of the total stretch, similar results to Figs. 6.16 or 6.17 are observed - the reader only need to sum up the percent cold and hot stretch. In doing so, the total stretch values expressed in Figs . 6.16 are 140, 160, and 180 percent while those for Figs. 6.17 are 100, 115, 130, and 140 percent. The Gurley numbers corresponding to the stretched films with their total extension values are displayed in Table 6.8 along with other cold and hot stretch combinations (the %TS values for the respective films are tallied in the top left corner of each cell). With one exception, the F1 membranes presented in this table are characterized as "quality" microporous films. The reader may recall that as the percent cold stretch (or %HS) increased for a constant hot stretch (or %CS), a lower Gurley number resulted. Thus, it was expected and indeed realized that the lowest Gurley values occurred for stretched films where both parameters (%CS & %HS) were maximized. The effect on morphology, as viewed by AFM, is shown for the two extremes of 100 and 180 percent total stretch in Figs. 6.20 a & b, respectively. Clearly, there is an observable difference in pore size between the two films, as measured along the MD, where the film produced with the larger total stretch is characterized by a larger pore size. Note that the micrograph displayed in Figs. 6.20b is the microporous morphology for the F1 film possessing the lowest Gurley (highest porosity) of any film prepared during this study.

Table 6.8 The Gurley number results from F1 microporous films which were a product of different %CS and %HS combinations. The %TS is displayed in the top left corner of each cell. The other annealing/stretching parameters remained constant with the standard condition.

%CS (%Extension)

%HS (%Extension)	50	70	90
50	100% 113 ± 12 sec	120% 96 ± 4 sec	140% 90 ± 5 sec
65	115% 92 ± 2 sec	135% 89 ± 7 sec	155% 78 ± 3 sec
80	130% 84 ± 6 sec	150% 82 ± 2 sec	170% 69 ± 4 sec
90	140% 83 ± 4 sec	160% 76 ± 3 sec	180% 63 ± 3 sec

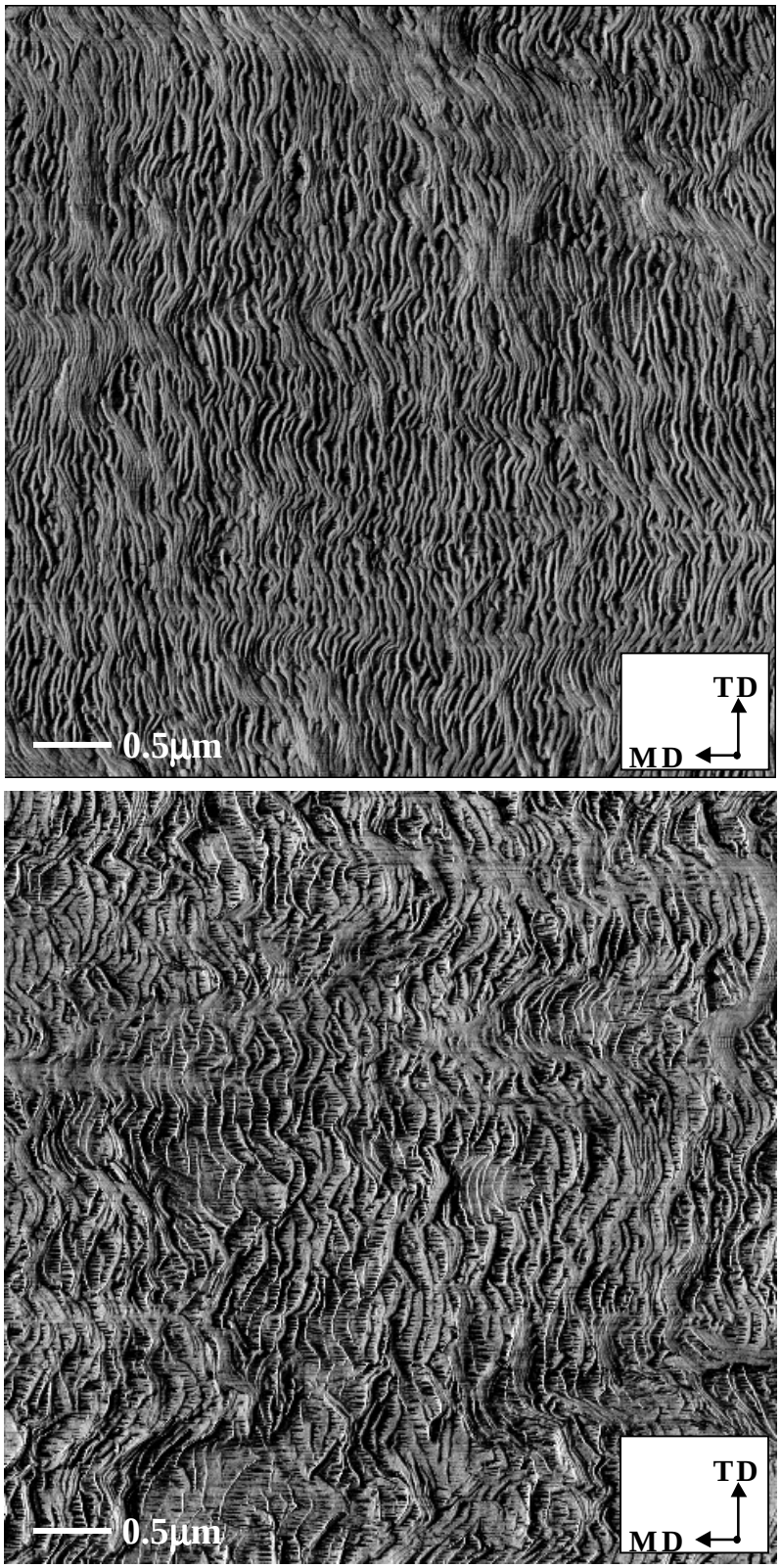

Figure 6.20 AFM phase images displaying the influence of %TS on F1 membrane morphology: a) %TS = 100% and b) %TS = 180%. The MD is labeled, and the images are each 5 μm x 5μm.

In a similar manner to the resin F films, precursor D1 was annealed and stretched using different parameter combinations. However, the resulting morphology and permeability were, as expected, dramatically different due to differences in the starting precursor morphology and crystalline orientation. Figure 6.21 provides an AFM micrograph of a D1 final stretched sample produced using the standard annealing/stretching conditions. It is evident that this D1 stretched film is absent of *any* microporous structure and analogous results were observed for *all* other annealing and stretching combinations concerning the resin D films. Thus, no further results addressing the resin D stretched films will be presented.

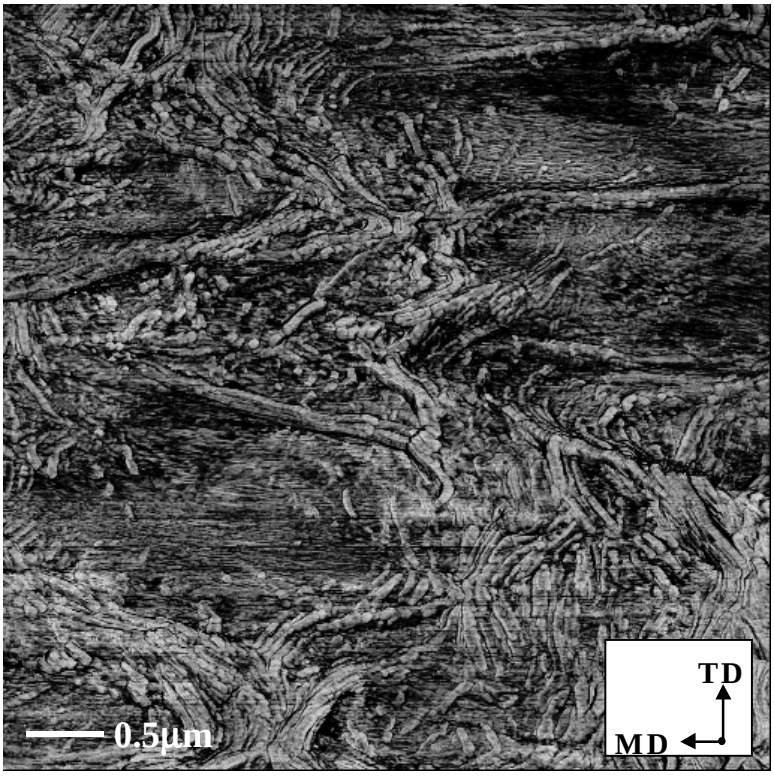

Figure 6.21 AFM phase image of the D1 stretched film utilizing the standard annealing/stretching condition. The MD is labeled, and the image is 5µm x 5µm.

6.4 DISCUSSION

The annealing results presented displayed that many physical properties of the annealed film including morphology, lamellar thickness and its distribution (as related to long spacing), and the degree of crystallinity (X_c) are controlled to varying degrees by the annealing temperature (T_a), time (t_a), and tension level. The application of uniaxial tension at lower annealing temperatures was found to produce interlamellar voids on the order of nanometers in size, as viewed by AFM. Thus, the main deformation process appeared to be lamellar separation. These findings were further supported by the use of SAXS on these samples, where a long spacing of ca. 13-14nm was measured. Upon increasing the isothermal annealing temperature above 130°C, the long spacing values for the films annealed under tension were similar to those observed for free-annealed specimens. Additionally, as the specific tension level utilized during annealing was increased, the scattering intensity (**I(s)**) of the 1st order peak for the corresponding sample diminished but did not shift with respect to **s** (i.e. **s*** did not change). These results suggest that the lamellae were possibly tilted away from the MD but still retained their dimensions. This conclusion is based upon previous studies regarding the deformation behavior POM spherulitic morphologies[14] as well as the earlier AFM results. In the present samples, lamellar tilting was observed via AFM for any annealed sample as long as elevated temperatures ($T_a \geq 130$°C) with higher tension levels (ca. 9-15%) were utilized. Further discussion of the SAXS results for the free-annealed specimens will be given later. Lamellar separation was therefore not the main deformation mode upon the application of higher tension levels (≥ 3%) at higher annealing temperatures ($T_a \geq 130$°C). Instead, inter and intra-lamellar slip as well as shear appears to be the main deformation modes accounting for the lamellae tilting.

The transition between different deformation modes with draw is not necessarily a novel finding for POM. O'Leary and Geil[14] previously reported deformation results with respect to POM materials possessing quiescently crystallized spherulitic morphologies. However, analogies can be drawn between their results and the stacked lamellae morphologies presented here. Specifically, comparisons can be made in the equatorial spherulitic regions, where the lamellae are stacked with their long directions perpendicular to the draw direction. In these regions, the lamellae should behave similar to our stacked lamellar morphologies. In fact, it was the equatorial regions that the following observations of O'Leary and Geil transpired. In their report, they noted that the transition from void formation to no void formation with draw occurred at a temperature of approximately 130°C using a rate ca. 5 mm/min. Below 130°C, these authors noted that voids formed in regions where the deformation was perpendicular to the

lamellae while above this temperature voids did not occur. Structurally, at elevated temperatures (>130°C), the long direction of the lamellae in these equatorial regions tilted towards the draw direction with increasing draw. In fact, the lamellae were observed to preferentially tilt approximately 30° into the draw direction. From this, they concluded that the chain axes within the lamellae lie at roughly this same angle to the lamellae normal (30°). They also reported that the lamellar tilting is further accompanied by lamellar breakup into slightly smaller units that are still much larger than any fibrillar-like structures. Thus, in our well-defined stacked lamellar materials, the main deformation mode is inter/intra lamellae with the application of tension at the higher annealing temperatures. Yet, as the annealing temperature is decreased, lamellar separation becomes the dominant deformation mode.

The findings of O'Leary and Geil are also helpful to explain the effect of tension on the "c" and "a"-axis orientation along MD. The reader may recall, that as the specific tension level increased, the corresponding "c" and "a"-axis orientations along MD decreased. In fact, the latter was absent in samples annealed under 15 percent tension. O'Leary and Geil further suggested that inter and intra-lamellae slip occurs along the chain axis, specifically along the (100) slip plane. They also proposed that as the deformation level increased, the twisting period decreased for lamellae at right angles to the draw direction. Eventually, lamellar discontinuities (i.e. lamellar fracture) were produced at sufficiently high deformation levels where the lamellae fracture in the twisted portion. Thus, smaller lamellae were produced essentially absent of twisting.[15] This explanation accounts for the observed loss of "a"-axis orientation along MD at higher tension levels, recall Fig. 6.11. The chains that composed these twisted portions initially contribute to the decrease in f_c orientation, i.e. decreased azimuthal dependence of the (100) reflection. Additionally, it is probable that many chains within the tilted lamellae are still parallel to the lamellar normal given the low levels of extension utilized. Such a result would further contribute to the decrease in the crystal orientation. It is speculated, however, that for greater levels of draw than those investigated here, the chains might well be sufficiently realigned with the MD to produce a higher WAXS azimuthal dependence than observed.

A number of these morphological and structural results are a consequence of an α_c relaxation present in POM. Recall that the range of temperatures encompassing the resin F α_c relaxation, as measured via DMA at 1 Hz, is approximately 40-165°C. Thus, as the annealing temperature increased from 85 to 150°C, the α_c relaxation was more activated. Upon applying tension at the higher annealing temperatures, the polymer chains were able to translate through the crystal more readily. The result is that at the lower temperature of 110°C, the lamellae behaved more

solid-like (less chain-slippage through the lamellae) and thus the main deformation mode was lamellar separation, rather than chain slip with lamellar tilting. The end result was more pores and less of a change in f_c versus films annealed at 145°C under tension.

The presence of a α_c relaxation in POM also accounts for the X_c increase and Δw decrease as annealing time or temperature was increased. In fact, similar findings for other polymers possessing an α_c relaxation[6,15-17] have been observed. Also recall the T_m was not systematically affected while the annealing temperature and time did influence the long spacing. In conclusion with regard to the annealing behavior of POM, the time spent in the range of temperatures encompassing the POM α_c relaxation and the temperature at which this time is spent are two factors that influence the resulting X_c, ℓ, and Δw.

We postulate that a more uniform and thicker crystalline phase, as a result of higher annealing temperatures and/or long annealing times, translates into a more permeable stretched film with higher observable amounts of microporosity. However, if the annealing temperature becomes too high (150°C), permeability begins to decrease. It is speculated that this possibly is a result of macroscopic lamellar melting during annealing, which would not be beneficial to lamellar splaying upon stretching. This was supported by Fig. 6.22, an AFM micrograph of a free-annealed F1 film using T_a equal to 150°C for 20min, where partial lamellar melting was recognized on the film surface. Since there is only a small difference in membrane permeability for stretched films annealed at 145°C versus 150°C for similar stretching conditions, the surface melting effect is not large.

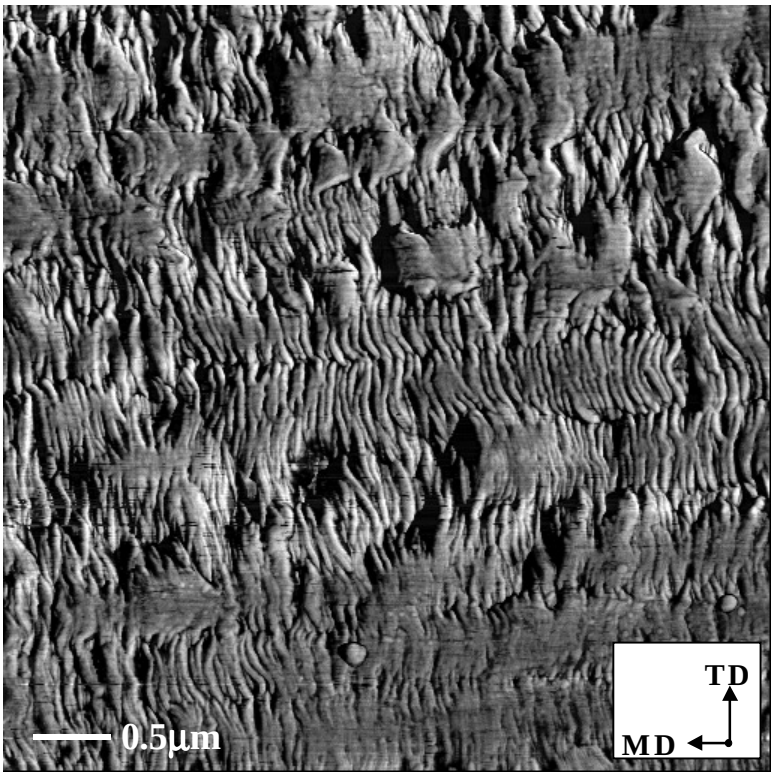

Figure 6.22 AFM phase image of the F1 free-annealed film utilizing a T_a = 150°C for 20min. The MD is labeled, and the image is 5μm x 5μm.

For the production of microporous films utilizing the MEAUS process, the desired deformation mode during stretching (third stage) is lamellar splaying. According to Peterlin and coworkers[18], this mode is initially the result of ductile drawing between the crystalline lamellae in the disordered amorphous phase using a slow strain rate and sufficient temperature. Thus, the cold stretch temperature must be sufficiently high to provide enough thermal energy enabling cooperative segmental mobility within the *amorphous* phase. Precisely, this temperature (T_{cs}) must be greater than the T_g for a specific polymer. In the case of POM, the glass transition temperature is disputed within the literature[15], however, both temperatures (ca. 0 and -70°C) thought to be attributed to T_g occur below room temperature. For all the temperatures utilized here during cold stretching, sufficient *amorphous* mobility should therefore be achieved. However, it is speculated that at the high levels of crystallinity present in the POM annealed films, higher T_{cs} values are required to provide adequate mobility for the initial ductile drawing of the amorphous phase. Why then does the permeability decrease for membranes cold stretched at 70°C versus those stretched at 50°C? This is attributed to *crystalline* mobility, which is more activated at 70°C versus 50°C. Thus, the lamellae behave less solid-like with greater chain translation occurring,[6] resulting in less micropore nucleation at the higher temperature.

In contrast to the cold stretching step, chain slippage is exactly the desired outcome in hot stretching, which is facilitated by a sufficiently high temperature during this step. For the resin F films, a hot stretch temperature of 100°C produced the lowest final film permeability. The reader may recall that the stretched film permeability levels decreased if the hot stretch temperature was increased above this value. Thus, during hot stretching at elevated temperatures (≥ 130), there is likely too much crystalline mobility and crystalline melting is occurring. However, these explanations are pure conjecture as there is no direct evidence.

The explanation accounting for the permeability and observable pore size dependence on the percent cold or hot stretch is quite evident. Larger cold stretch extension levels "nucleate" greater numbers of pores that become enlarged during hot stretching as the extension level is increased. This also translates into larger percent total stretch values producing more permeable membranes with larger micropores as was observed in Fig. 6.20. As previously discussed, cold and hot stretching must be executed at the proper temperatures in order to produce the desired outcome. From the above results and discussion, the general film permeability dependence on the annealing and stretching parameters was recognized. In fact, a resin F final film possessed the highest permeability if it was free-annealed at 145°C for 20 min. followed by cold stretching

at a temperature of 50°C to 90 percent extension and then hot stretched at 100°C to an extension level of 90 percent. Even when the Gurley values were normalized to final film thickness, this result still held.

The effect of precursor f_c and morphology has yet to be discussed although it was found to influence the membrane permeability. Specifically, it was discovered that a F1 stretched sample possessed a higher permeability than a F2 final film, when annealed and stretched under equal conditions. Recall that precursor F1 was characterized by a slightly more planar lamellar morphology and a higher f_c value with respect to the MD than the precursor F2 (0.81 versus 0.75, respectively). Therefore, starting film morphology and orientation state play an integral role on the final film properties. In most cases upon annealing and stretching the resin F precursors, microporous membranes were produced although to varying degrees for the processing window studied. This was not true for resin D films, which were also subjected to a large number of variable combinations similar to those applied to the resin F films. Once again, it was the precursor properties that are believed to be the cause, specifically the morphology. The reader may recall that precursor D1 possessed a sheaf-like twisted lamellar morphology with an f_c equal to 0.45.

From the above results and discussion, the criteria or recommended prerequisites by the authors for successfully converting a semicrystalline polymer by the MEAUS process into a microporous membrane appear to be correct. Reiterating, these prerequisites are:

1) "Fast" crystallization kinetics
2) A highly planar lamellae morphology (limited lamellar twisting) for the extruded precursor
3) "High" orientation of the crystalline phase in the precursor
4) Proper film thickness (1mil) and quenching rate to facilitate rapid heat transfer of the film to limit skin-core effects
5) Presence of a α_c relaxation.

Lastly, the annealing and stretching conditions must be optimized to attain the best permeability as has been shown for these POM films for the processing conditions studied.

6.5 CONCLUSIONS

This particular paper addressed the findings of the latter two stages (annealing and stretching) regarding the MEAUS process utilizing resins D and F. In terms of the annealing

effects on the films, the following conclusion can be made. As the values of T_a or t_a were increased, the magnitude of X_c and long spacing increased, which is attributed to the presence of crystalline mobility, associated with the α_c relaxation. The application of tension during annealing influenced whether the annealed film morphology did or did not possess voids, which also depended upon the annealing temperature utilized for tension levels greater than 3 percent.

The morphological alterations as a result of annealing impacted the final microporous morphology. Greater tension levels produced lower permeability as well as less typical porous morphologies, regardless of the other annealing or stretching conditions utilized. In contrast, greater membrane permeability was obtained when higher values of T_a and t_a were employed during annealing. The final film permeability also increased for greater extension levels during either the cold or hot stretching steps. Additionally, the stretching temperature (T_{cs} or T_{hs}) affected the microporosity and permeability. The initial melt-extruded morphology and f_c were also found to be influential regarding the microporosity and permeability of the final film. In fact, the lower f_c value and slightly twisted lamellar morphology are believed to be the main reason why the precursors from resin D were not able to form microporous membranes.

Acknowledgements

The authors would like to thank the Celgard Corporation LLC for their continuing financial assistance for this project as well as the informative discussions that have taken place with them. Also, the authors thank Stephen McCartney for aiding in the instruction of AFM.

References

[1] Johnson, M. B., Wilkes, G. L., PMP extrusion paper submitted for review in *JAPS*.
[2] Johnson, M. B., Wilkes, G. L., PMP annealing/stretching paper submitted for review in *JAPS*.
[3] Johnson, M. B., Wilkes, G. L., POM extrusion paper submitted for review in *JAPS*.
[4] Druin, M. L., Loft, J. T., Plovan, S. G., U. S. Patent 3,801,404, 1974, assigned to Celanese Corp.
[5] Boyd, R. H., *Polymer*, **26**, 323, (1985); **26**, 1123, (1985).
[6] Rault, J., J.M.S.- Rev. Macromol. Chem. Phys., **C37**(2), 335, (1997).
[7] Marand, H., Xu, J., Srinivas, S., *Macromolecules*, **31**, 8219, (1998).
[8] Garber, C. A., Clark, E. S., *J. Macromol. Sci.-Phys.*, **B4**(3), 499, (1970); *Int. J. Polym. Mater.*, **1**, 31, (1971).
[9] Quynn, R. G., Brody, H., *J. Macromol. Sci.-Phys.*, **B5**(4), 721, (1971).
[10] Odian, G., "Principles of Polymerization 3rd Edition", John Wiley & Sons, New York, 1991.
[11] Hermans, P. H., Hermans, J. J., Vermaas, D., Weidinger, A., *J. Polym. Sci.*, **3**, 1, (1947).
[12] Yu, T. H., Ph.D. Dissertation (advisor: G. L. Wilkes) Virginia Tech, 1995.
[13] Celgard Corporation LLC, Company product literature.
[14] O'Leary, K., Geil, P. H., *J. Macromol. Sci., Phys.*, **B2**(**2**), 261, (1968).
[15] McCrum, N. G., Read, B. E., Williams, G., "Anelastic and Dielectric Effects in Polymeric Solids", Wiley, New York, 1967.
[16] Popli, R., Mandelkern, L., Bension, R. S., *J. Polym. Sci., Polym. Phys. Ed.*, **5**, 407, (1984).
[17] Zhou, H., Wilkes, G. L., *Macromolecules*, **30**, 2412, (1997).
[18] Peterlin, A., Sakaoku, K., *J. Appl. Phys.*, **38**, 1967, 4152.